

7th IAA Planetary Defense Conference

26-30 April 2021, Online Event

Hosted by UNOOSA in collaboration with ESA



Session 7a: Deflection & Disruption Testing

Chairs: Patrick Michel | Angela Stickle | Megan Syal

Presenters: S. Raducan | R. Luther | R. Nakano |
P. King | N. Gentile

Cratering processes on rubble-pile asteroids: insights from laboratory experiments and numerical models

S.D. Raducan¹, J. Ormö², M.I. Herreros², K. Wünnemann^{3,4}, Y. Zhang⁶, R. Luther³, C. Hamann³, G.S. Collins⁵, P. Michel⁶ and M. Jutzi¹

¹Space Research and Planetary Sciences, Physikalisches Institut, University of Bern, Switzerland; ²Centro de Astrobiología (INTA-CSIC), Torrejon de Ardoz, Spain; ³Museum für Naturkunde Berlin, Leibniz Institute for Evolution and Biodiversity Science, Germany; ⁴Freie Universität Berlin, Germany; ⁵Impacts and Astromaterials Research Centre, Department of Earth Science and Engineering, Imperial College London, UK; ⁶Université Côte d'Azur, Observatoire de la Côte d'Azur, Laboratoire Lagrange, France.

26-30 April 2021

7th IAA Planetary Defence Conference 2021



DART is a kinetic impactor test

DART = Double Asteroid Redirection Test

- S-type double asteroid system
- YORP asteroids \Rightarrow low cohesion and high porosity
- Diameter of the secondary: 150–180 m

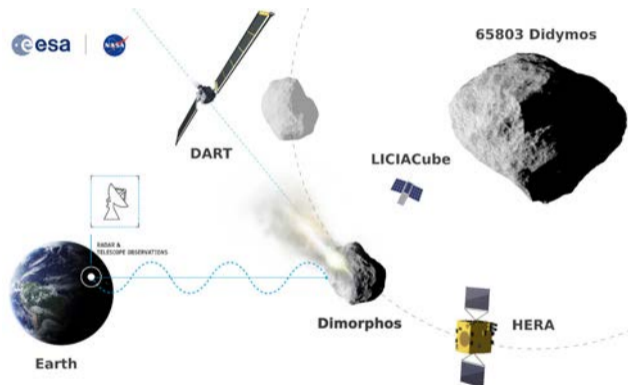


Figure 1: DART mission concept, at the point of impact. Source: ESA.

What do we know about the impact conditions and what is the main driver for β ?

Target properties



Figure 2: Dimorphos. Source: ESA.

Impact conditions

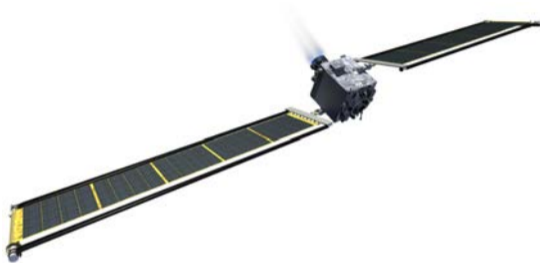


Figure 3: DART spacecraft. Source: NASA.

- Cohesive strength – **not known**
- Bulk density/porosity – **not known**
- Internal structure – **not known**

- Impact velocity – **known**
- Impact angle – **not known**
- Impactor mass/shape – **known**

Previous work quantifies the effects of various target properties and simple structures ($Y_0 > 100$ Pa)

The DART impact into different targets can produce the same β , but different craters. Both β and crater size/morphology together can be diagnostic of target properties (Raducan et al., 2020).

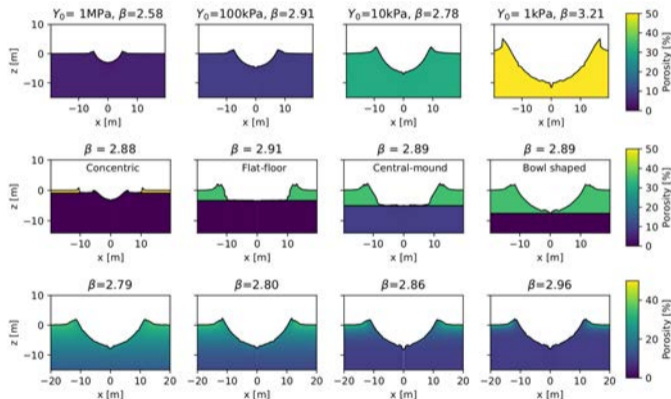


Figure 4: Crater profiles from iSALE-2D simulations of various targets.

Ryugu, Bennu – both rubble-pile asteroids. Dimorphos also a rubble-pile?

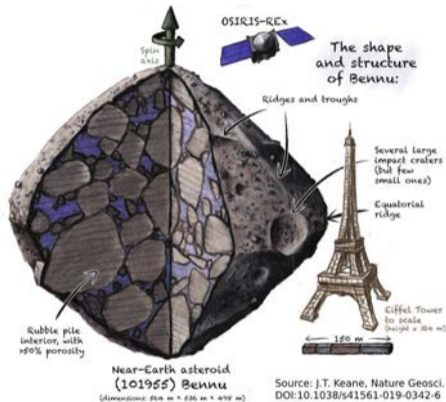
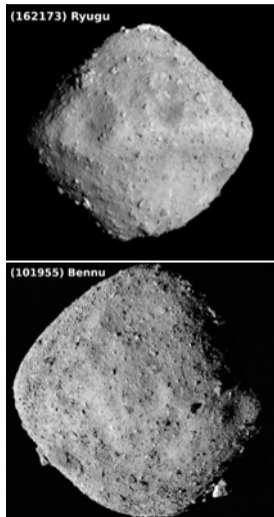
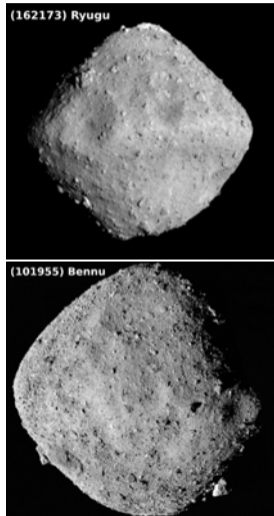


Figure 5: Sketch of asteroid Bennu interior. Source: James Tuttle Keane, Nat. Geosci. vol. 12 (226).

Ryugu, Bennu – both rubble-pile asteroids. Dimorphos also a rubble-pile?



We need to validate our numerical models against laboratory experiments!
We need laboratory experiments purposely designed to mimic asteroid surfaces!

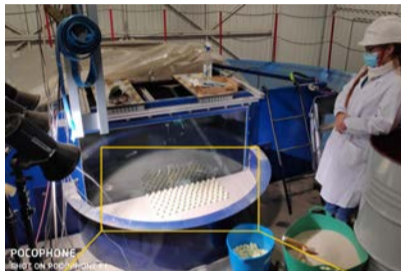
Experimental Projectile Impact Chamber (EPIC) - Quarter space experiments into heterogeneous targets

Projectile:

- Delrin (disrupts upon impact), 2 cm diameter, $m_p = 5.7$ g
- Velocity: ≈ 400 m/s

Target:

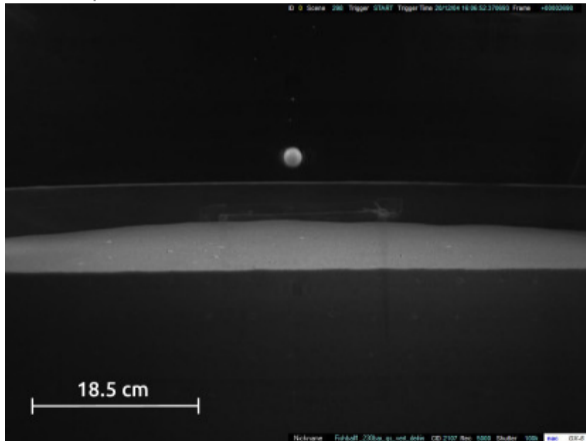
- 4 layers of porous ceramic balls embedded in dry beach sand matrix;
- Sand: $\rho = 1.8$ g/cm³;
- Ball: $d = 2.25$ cm, $m = 5.7$ g, $\approx 50\%$ porosity.



We used SPH to model the EPIC experiment

$T = 0$ ms

EPIC experiment



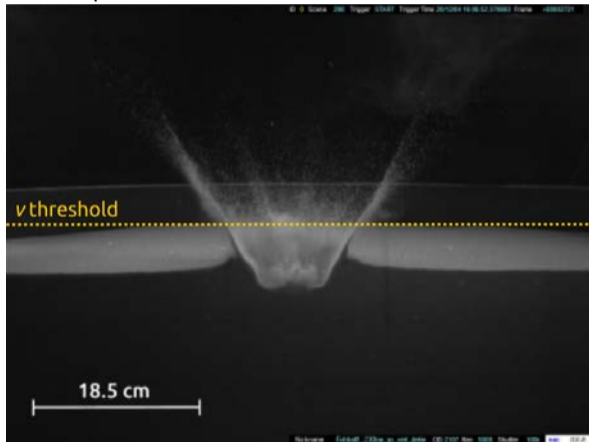
SPH simulation (only slow ejecta)



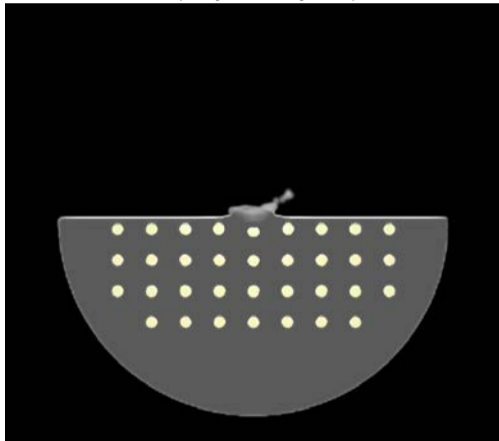
We used SPH to model the EPIC experiment

$T = 4 \text{ ms}$

EPIC experiment



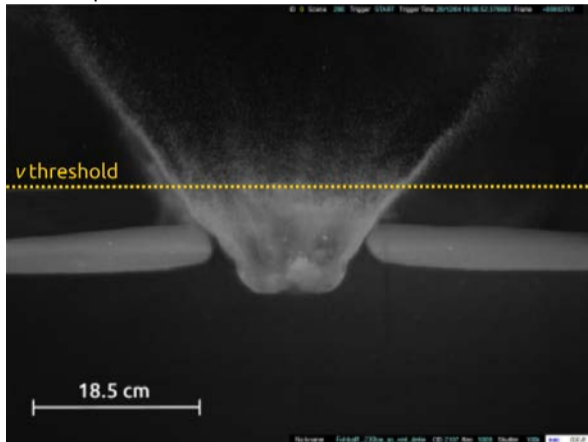
SPH simulation (only slow ejecta)



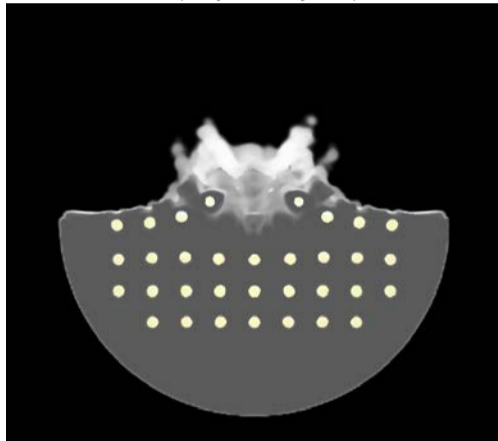
We used SPH to model the EPIC experiment

$T = 10$ ms

EPIC experiment



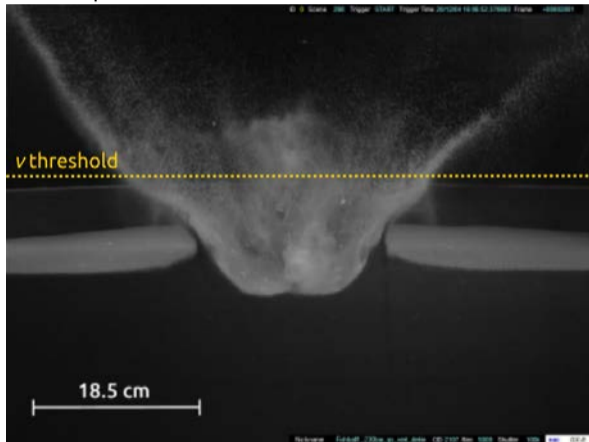
SPH simulation (only slow ejecta)



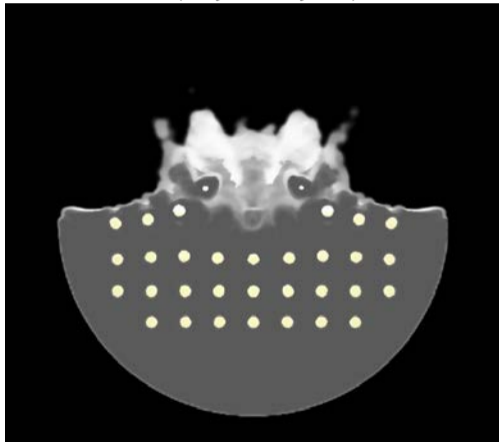
We used SPH to model the EPIC experiment

$T = 20 \text{ ms}$

EPIC experiment



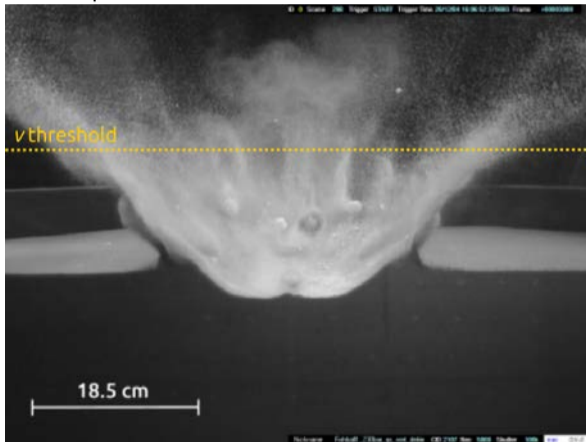
SPH simulation (only slow ejecta)



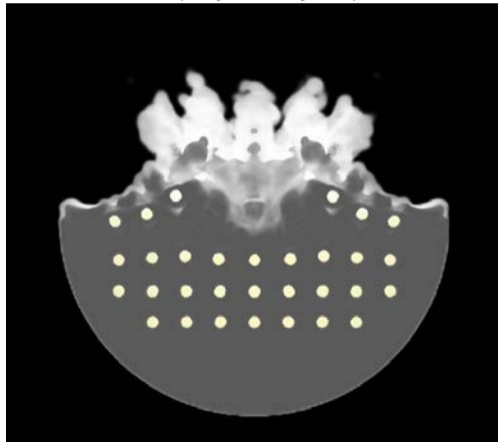
We used SPH to model the EPIC experiment

$T = 35 \text{ ms}$

EPIC experiment



SPH simulation (only slow ejecta)



We used SPH to model the EPIC experiment

Final crater - good match with the experiment

Crater dimensions

Pre-impact level diameter: 20.2 cm

Rim diameter: 28.2 cm

Depth: 2.9 cm

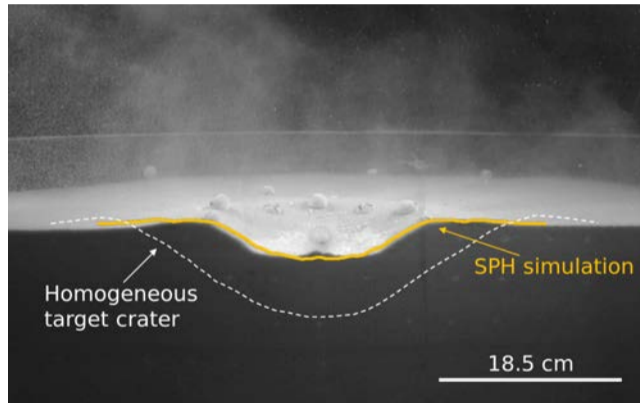


Figure 6: Final crater morphology ($T \approx 0.8$ s).

We used SPH to model the EPIC experiment

Boulder distribution - good match with the experiment

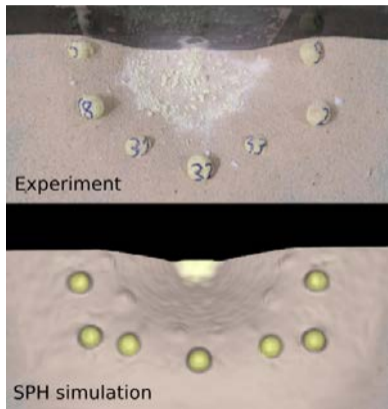
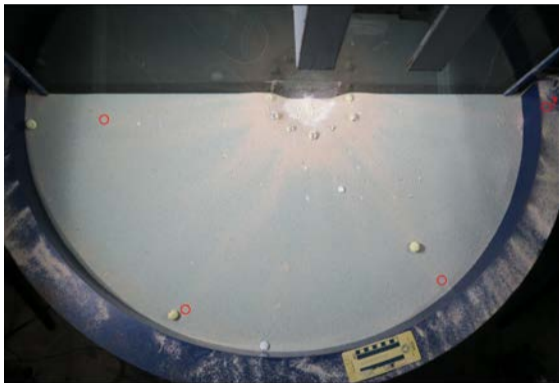
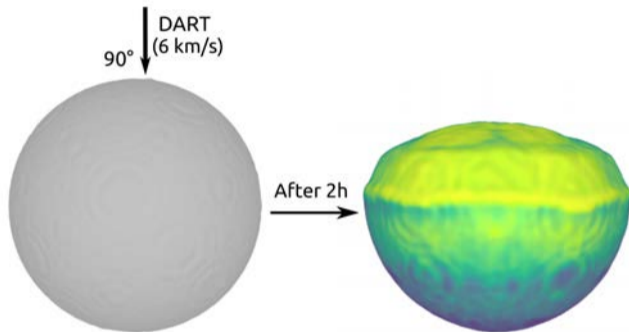


Figure 7: Boulder distribution.

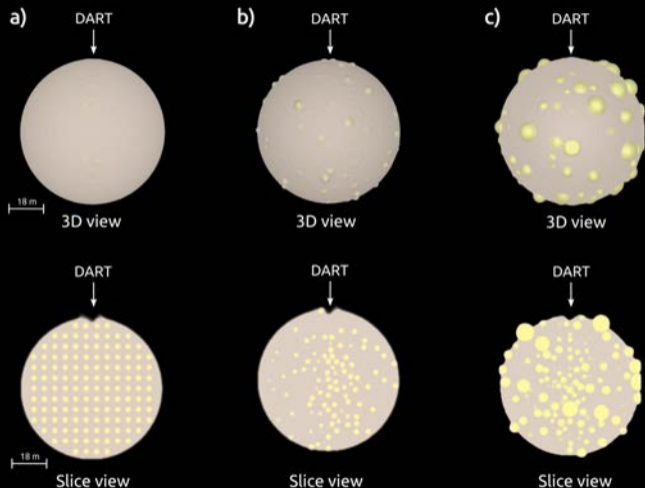
We used SPH to model DART-like impacts on spherical homogeneous asteroid



radius a (m)	Impactor mass m (kg)	velocity U (km/s)	strength Y_0 (Pa)	Target friction f	density ρ (kg/m ³)
0.5	500	6.0	0	0.6	1620

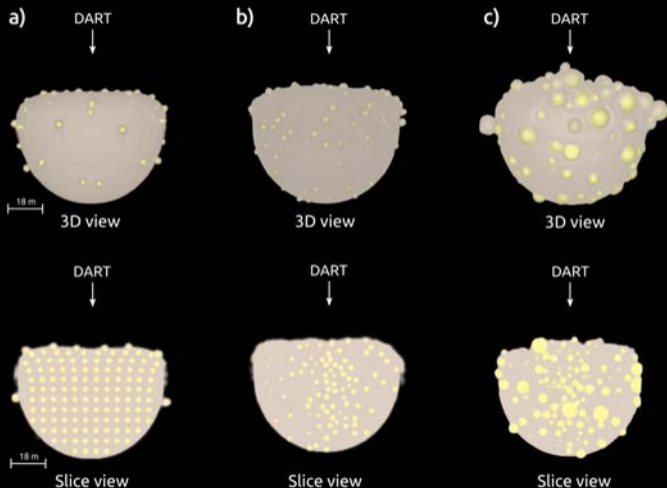
We modelled DART-like impacts on spherical rubble-pile asteroids - initial

- a) Grid-like distribution of 2.5 m boulders;
- b) Random distribution of 2.5 m boulders;
- c) Random distribution of boulders between 2 and 10 m.



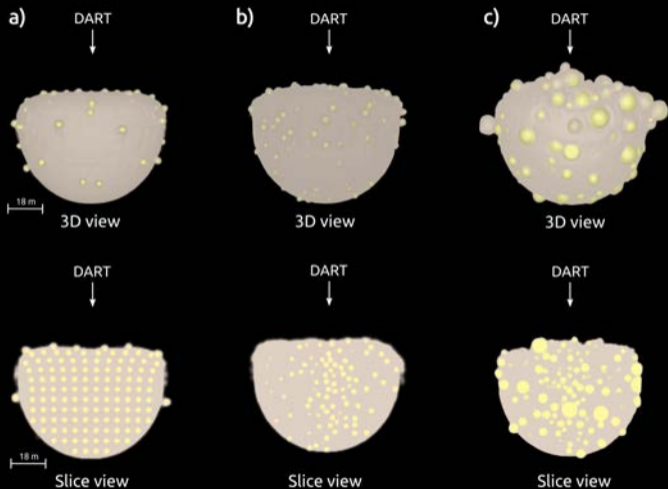
DART-like impacts on spherical rubble-pile asteroids – after ≈ 2 h

- a) Grid-like distribution of 2.5 m boulders;
- b) Random distribution of 2.5 m boulders;
- c) Random distribution of boulders between 2 and 10 m.



DART-like impacts on spherical rubble-pile asteroids – after ≈ 2 h

Homogeneous target



The boulder size-distribution influences the deflection efficiency, β

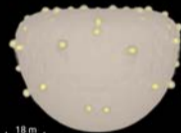
Homogeneous target



$\beta = 4.96$

a)

DART



3D view

$\beta = 3.33$

b)

DART

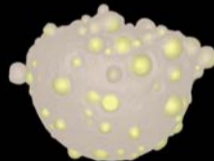


3D view

$\beta = 3.32$

c)

DART



3D view

$\beta = 3.83$

Conclusions

- The DART mission may impact a rubble-pile asteroid. We need laboratory experiments purposely designed to mimic asteroid surfaces;
- SPH simulations of impacts into heterogeneous targets show great agreement with laboratory experiment results;
- The DART impact on cohesionless spherical bodies is likely to produce morphologies that are dissimilar to cratering and change the global morphology of the asteroid;
- DART-like impact simulations on rubble-pile asteroids show that both the target morphology and the momentum transfer are affected by the distribution of surface boulders.

Acknowledgements



This project has received funding from the European Union's Horizon 2020 research and innovation programme, NEO-MAPP, under grant agreement No 870377.

JO was supported by grants ESP2014-59789-P, ESP2015-65712-C5-1-R and ESP2017-87676-C5-1-R from the MINECO and FEDER. JO and MIH were supported by the AEI Project No.MDM-2017-0737 INTA-CSIC and the CSIC support for international cooperation: I-LINK project LINKA20203.



This project has received funding from the European Union's Horizon 2020 research and innovation programme under grant agreement No 870377.

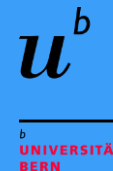


Near Earth Object
Modelling And Payloads
for Protection



Kinetic Impactor Technique: Benchmark and Validation Studies with iSALE and SPH

R. Luther, S.D. Raducan, M. Jutzi, K. Wünnemann, P. Michel,
Y. Zhang, D. Koschny, T.M. Davison, G.S. Collins
28.04.2021



Imperial College
London

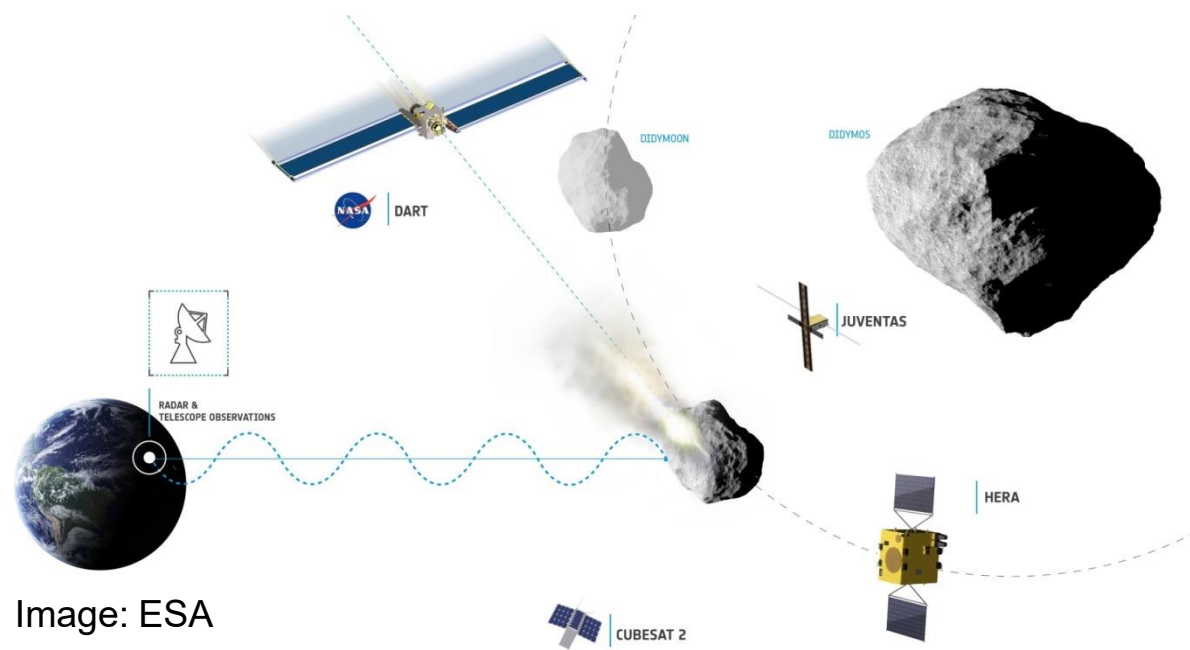
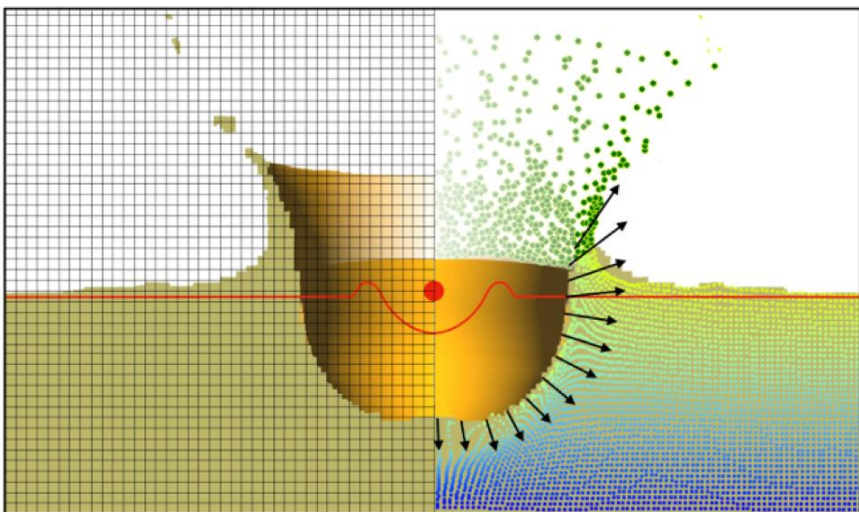


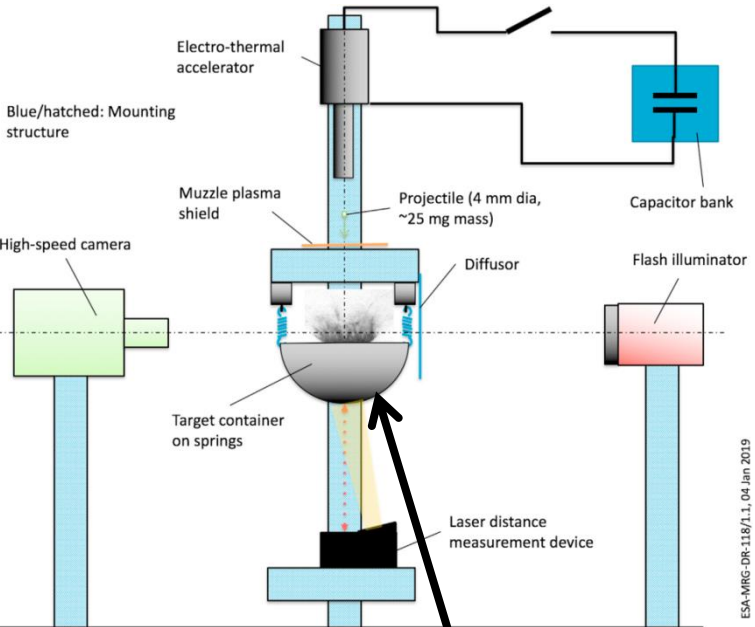
Image: ESA

- **Objective:** relate observed orbital change with momentum enhancement and crater morphology for given material properties (low strength regime)
- Shock physics codes simulate different materials; prove accuracy by:
 - validation against experiments
 - benchmarking codes (iSALE & SPH)

iSALE
(grid-based code)



SPH
(particle code)



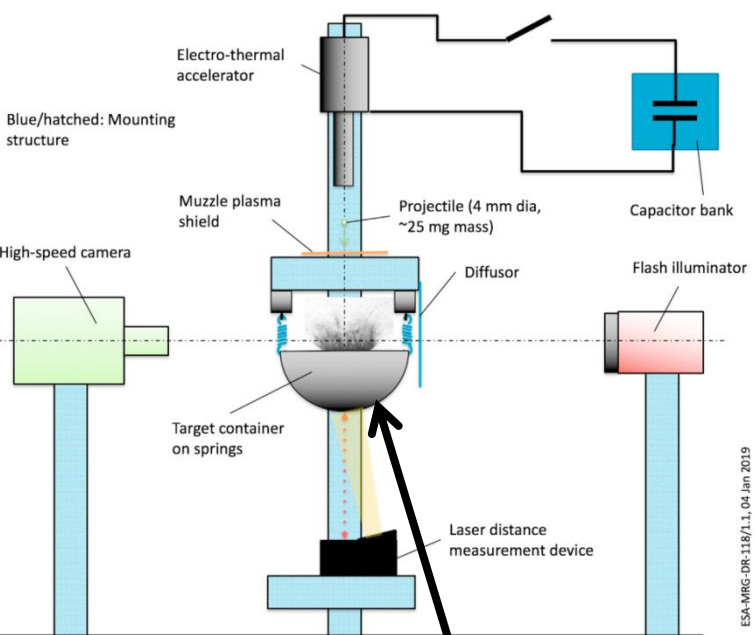
ESA-MRG-DR-118/1.1, 04 Jan 2019



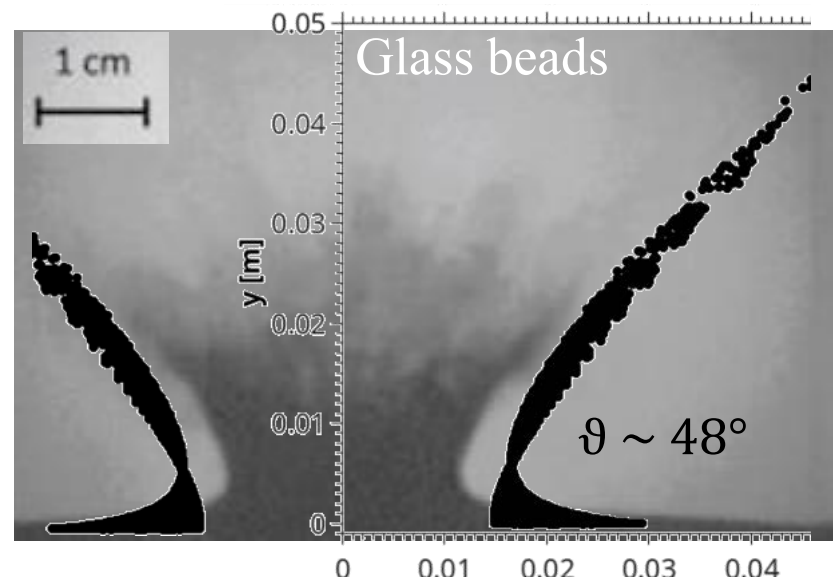
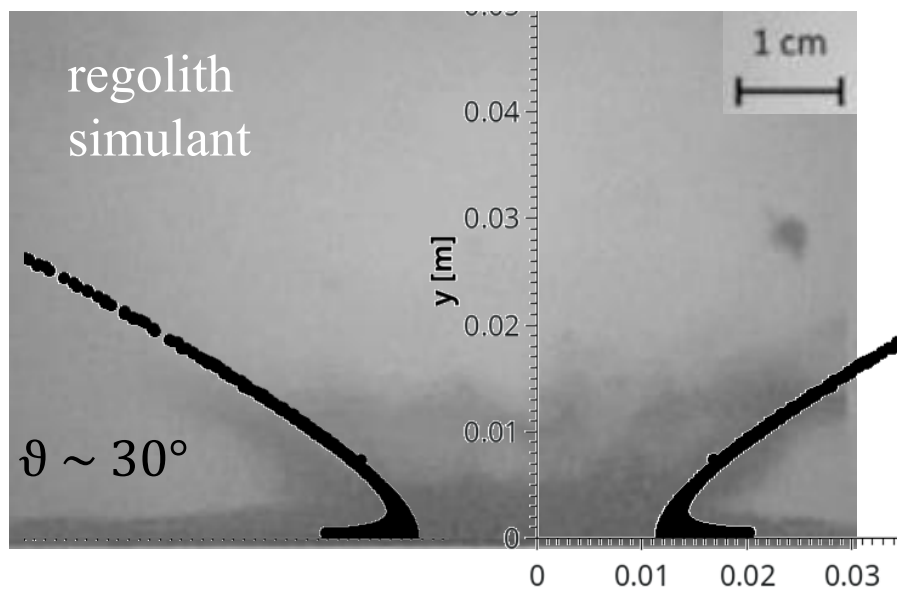
Experimental Setup:

- Chourey et al. 2020, PSS:
 - $v \sim 1-3$ km/s
 - target materials:
 - glass beads
 - quartz sand
 - regolith simulant
 - formation of ejecta curtain
 - crater size
 - momentum enhancement

Laboratory Experiments of Impacts into Regolith Simulant & Glass Beads



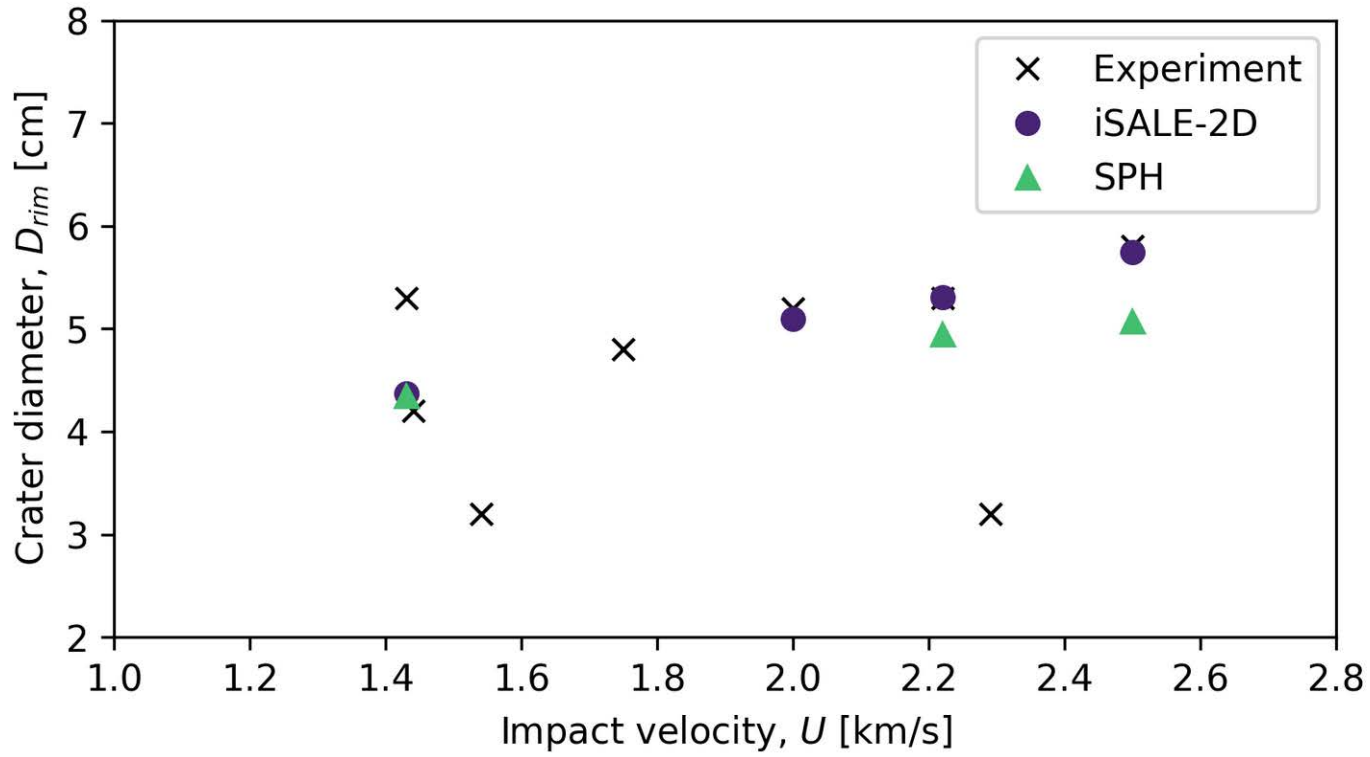
ESA-MRG-DR-118/1.1, 04 Jan 2019



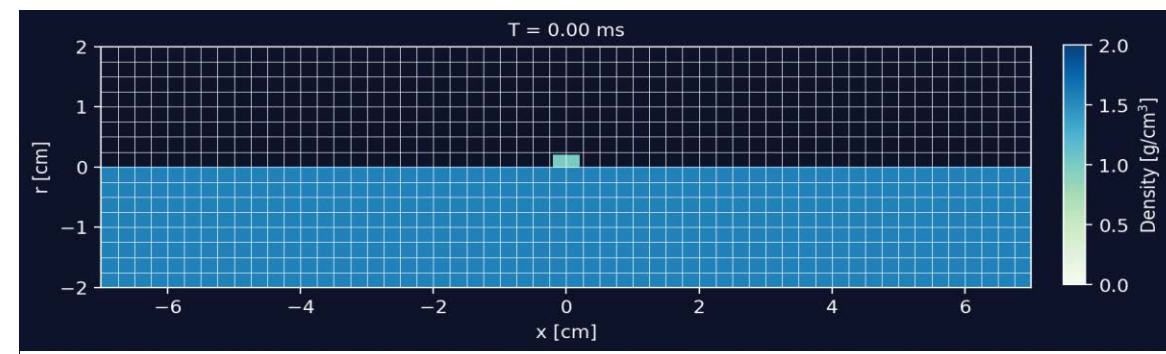
Experimental Setup:

- Chourey et al. 2020, PSS:
 - $v \sim 1-3$ km/s
 - target materials:
 - glass beads
 - quartz sand
 - regolith simulant
 - formation of ejecta curtain
 - crater size
 - momentum enhancement



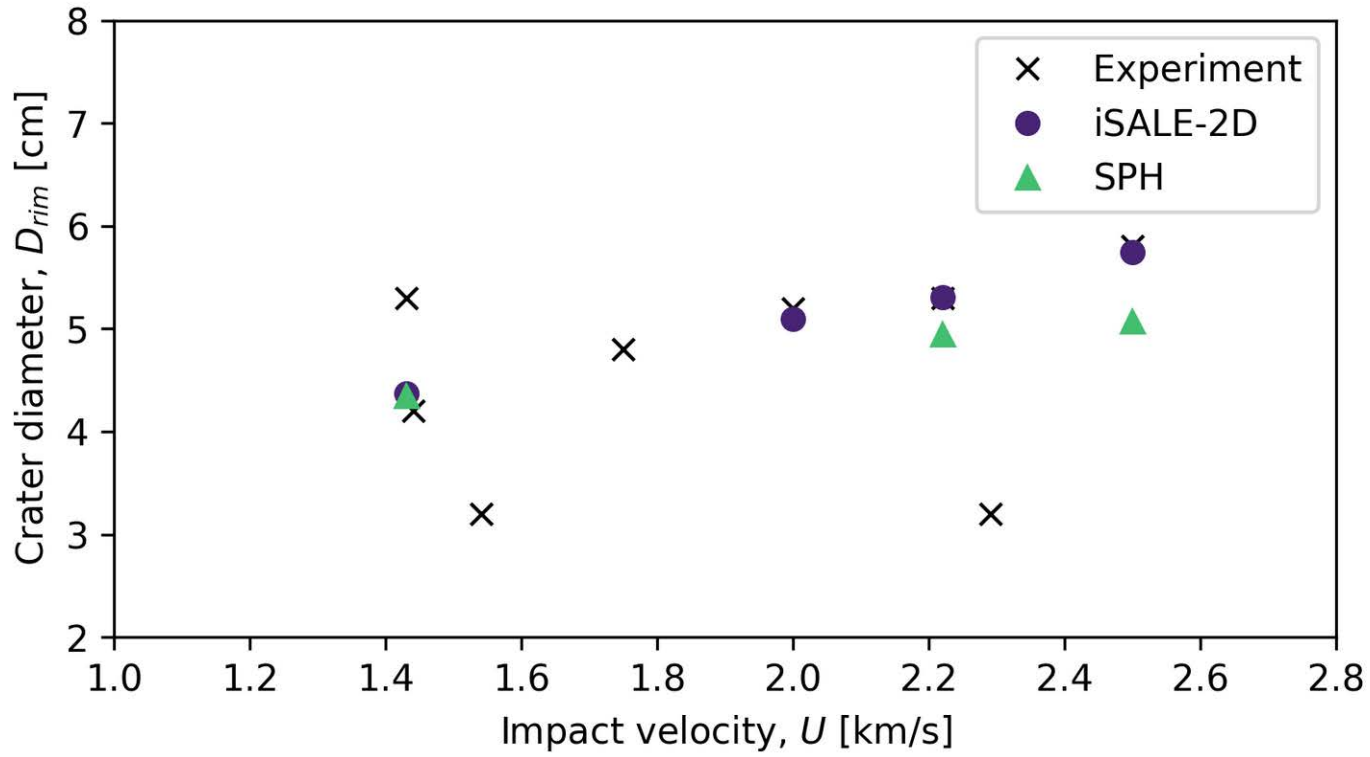


- similar material models & parameters for iSALE-2D and SPH
- both codes agree with experimental data
- some deviation towards faster impact velocity between codes

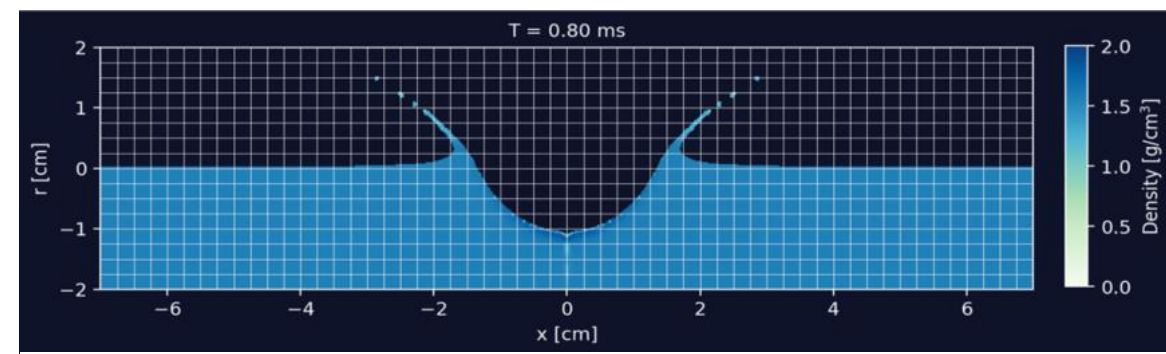


$v = 2.2$ km/s, $m = 24$ mg (PVC), regolith simulant
(experiment: Chourey et al. 2020, PSS)

Strength model	Lundborg, $Y_0=1.4$ kPa, $f=0.77$
Porosity model	ϵ - α -model (iSALE), $\kappa=0.96$
$\Phi=42\%$	P- α -model (SPH), $P_e=100$ Pa, $P_s=1.5$ GPa

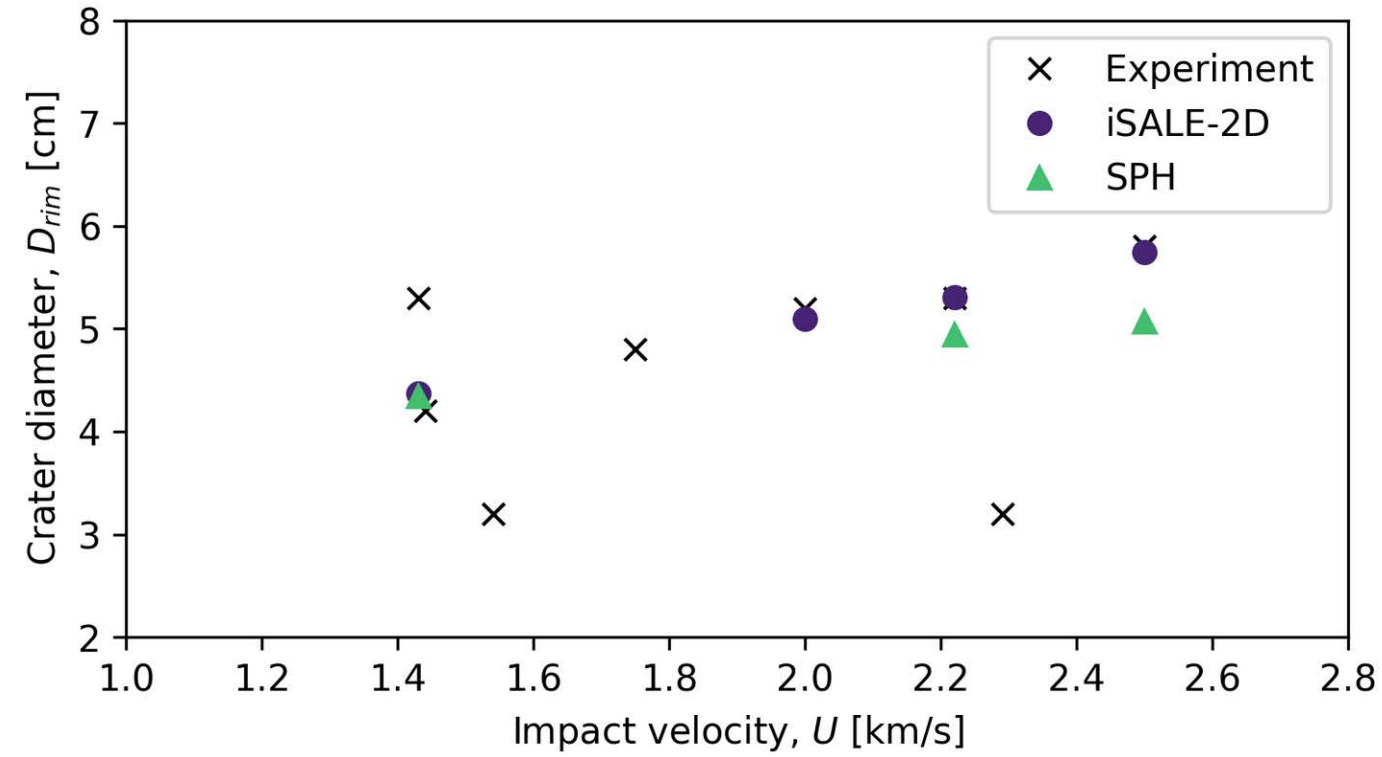


- similar material models & parameters for iSALE-2D and SPH
- both codes agree with experimental data
- some deviation towards faster impact velocity between codes

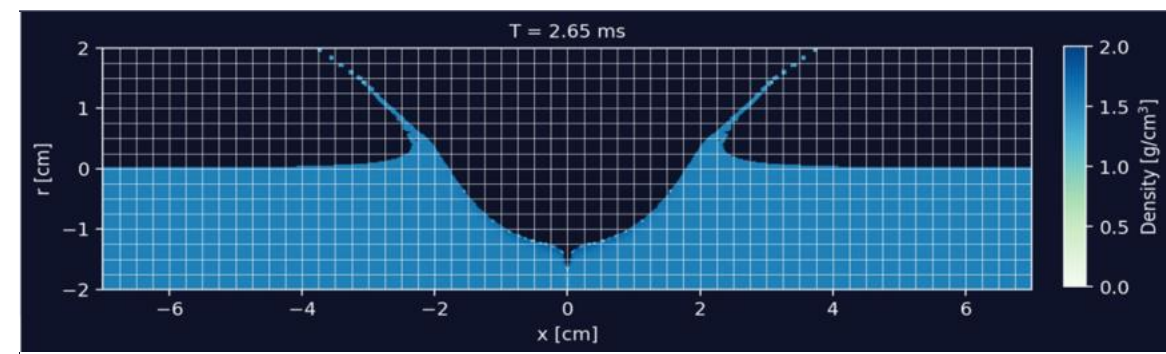


$v = 2.2$ km/s, $m = 24$ mg (PVC), regolith simulant (experiment: Chourey et al. 2020, PSS)

Strength model	Lundborg, $Y_0=1.4$ kPa, $f=0.77$
Porosity model	ϵ - α -model (iSALE), $\kappa=0.96$
$\Phi=42\%$	P- α -model (SPH), $P_e=100$ Pa, $P_s=1.5$ GPa

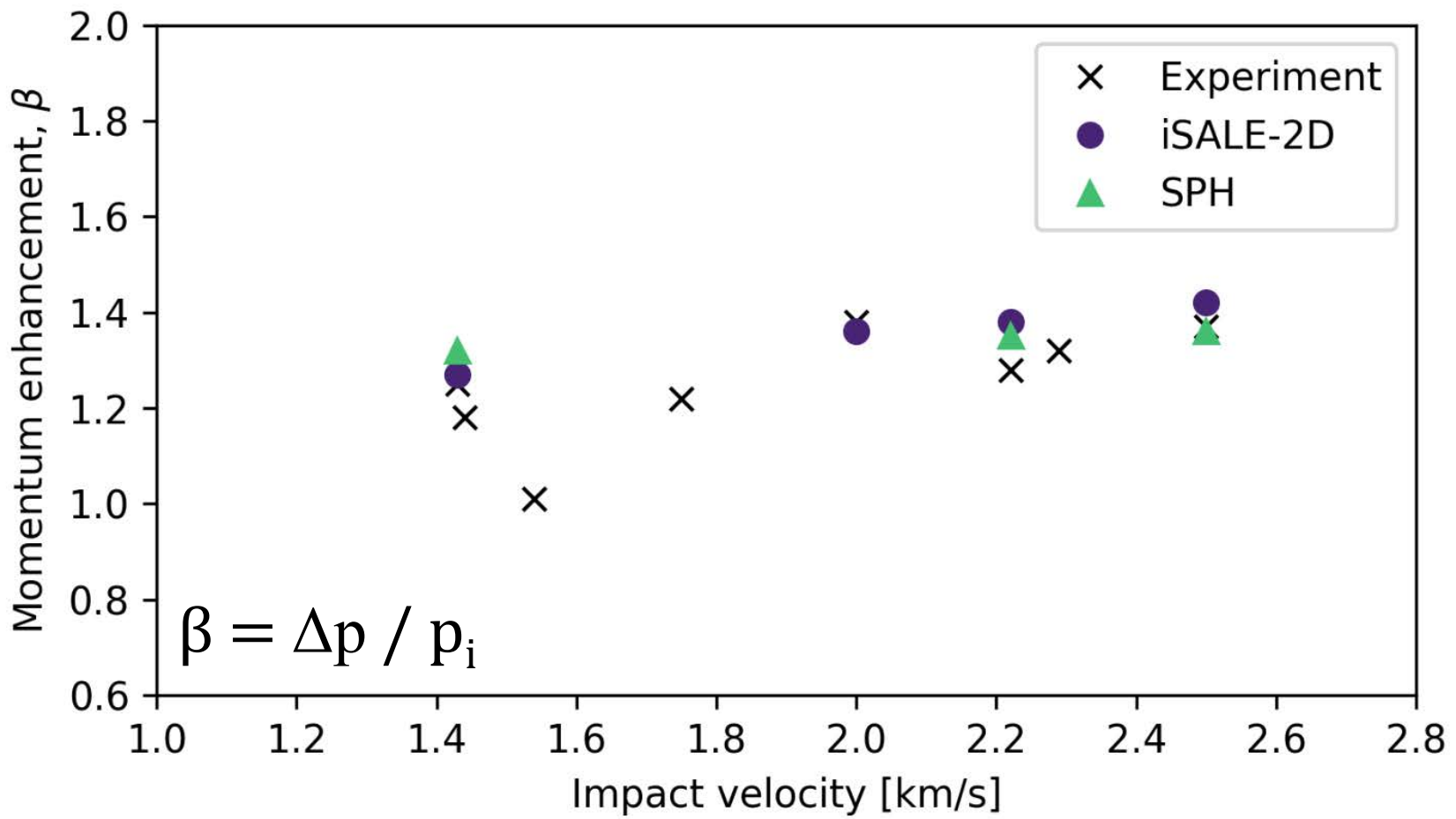


- similar material models & parameters for iSALE-2D and SPH
- both codes agree with experimental data
- some deviation towards faster impact velocity between codes



$v = 2.2$ km/s, $m = 24$ mg (PVC), regolith simulant
(experiment: Chourey et al. 2020, PSS)

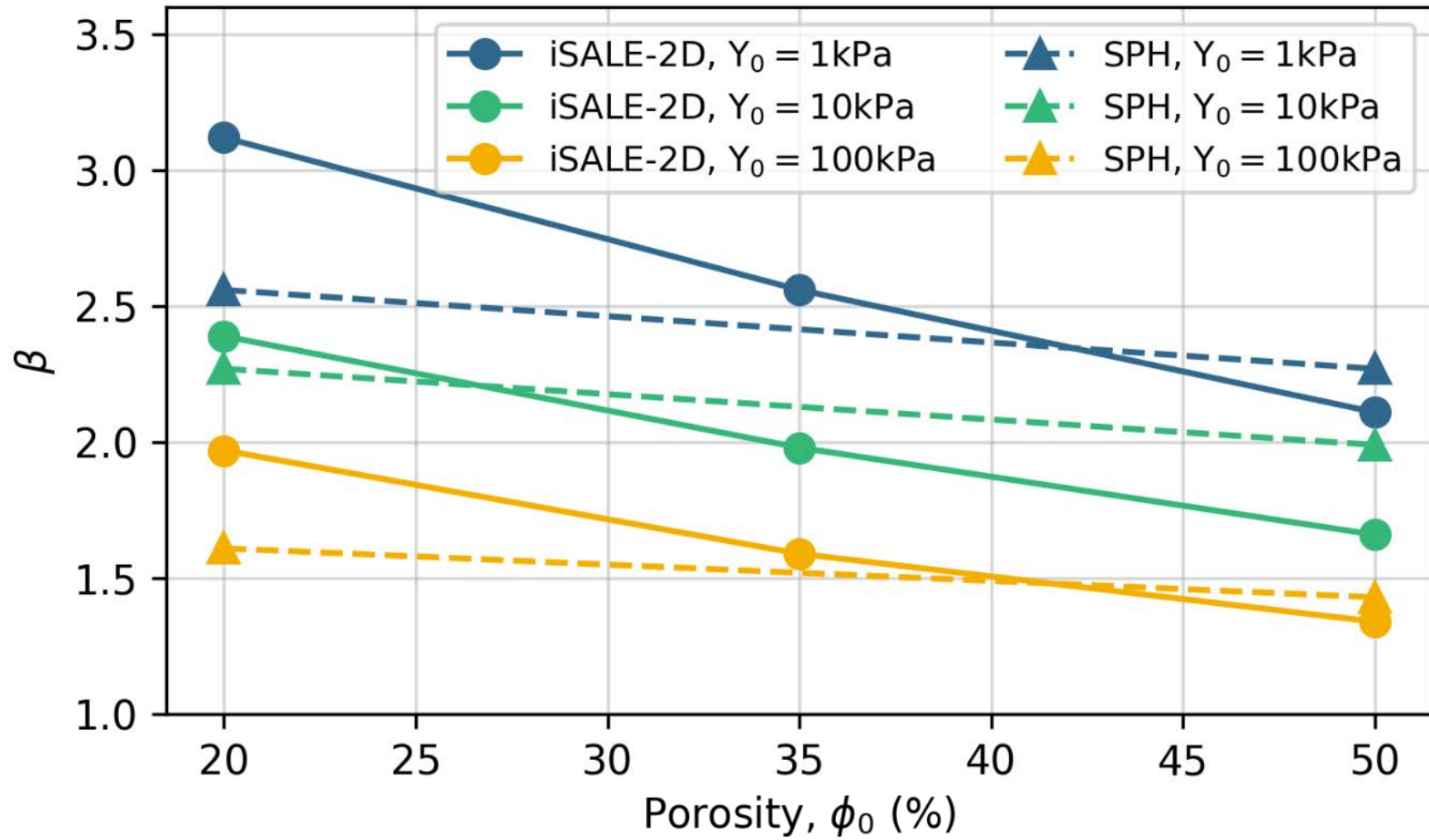
Strength model	Lundborg, $Y_0=1.4$ kPa, $f=0.77$
Porosity model $\Phi=42\%$	ϵ - α -model (iSALE), $\kappa=0.96$ P- α -model (SPH), $P_e=100$ Pa, $P_s=1.5$ GPa



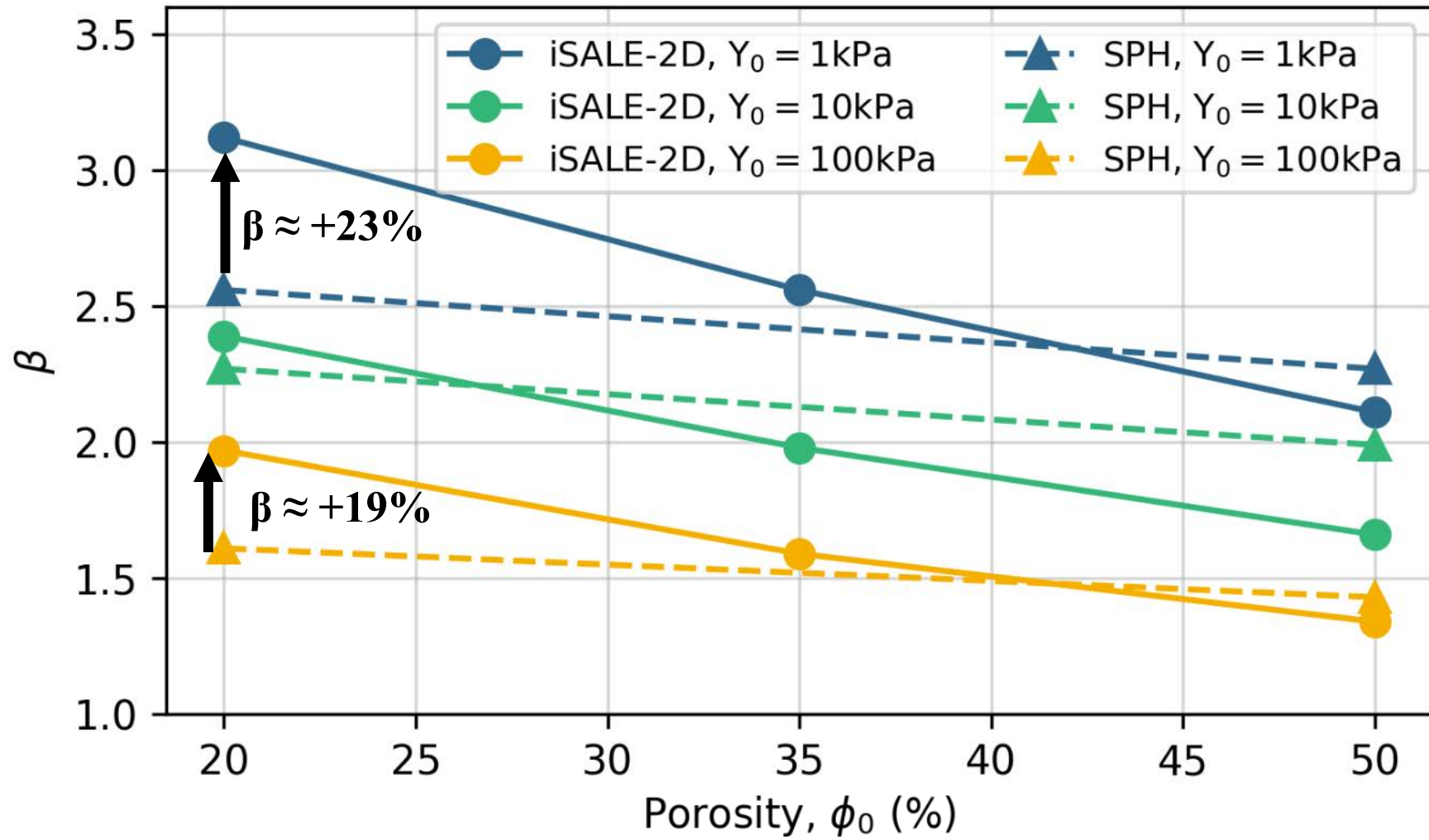
- similar material models & parameters for iSALE-2D and SPH
- both codes agree with experimental data
- results from both codes agree with each other

$$\beta = \Delta p / p_i$$

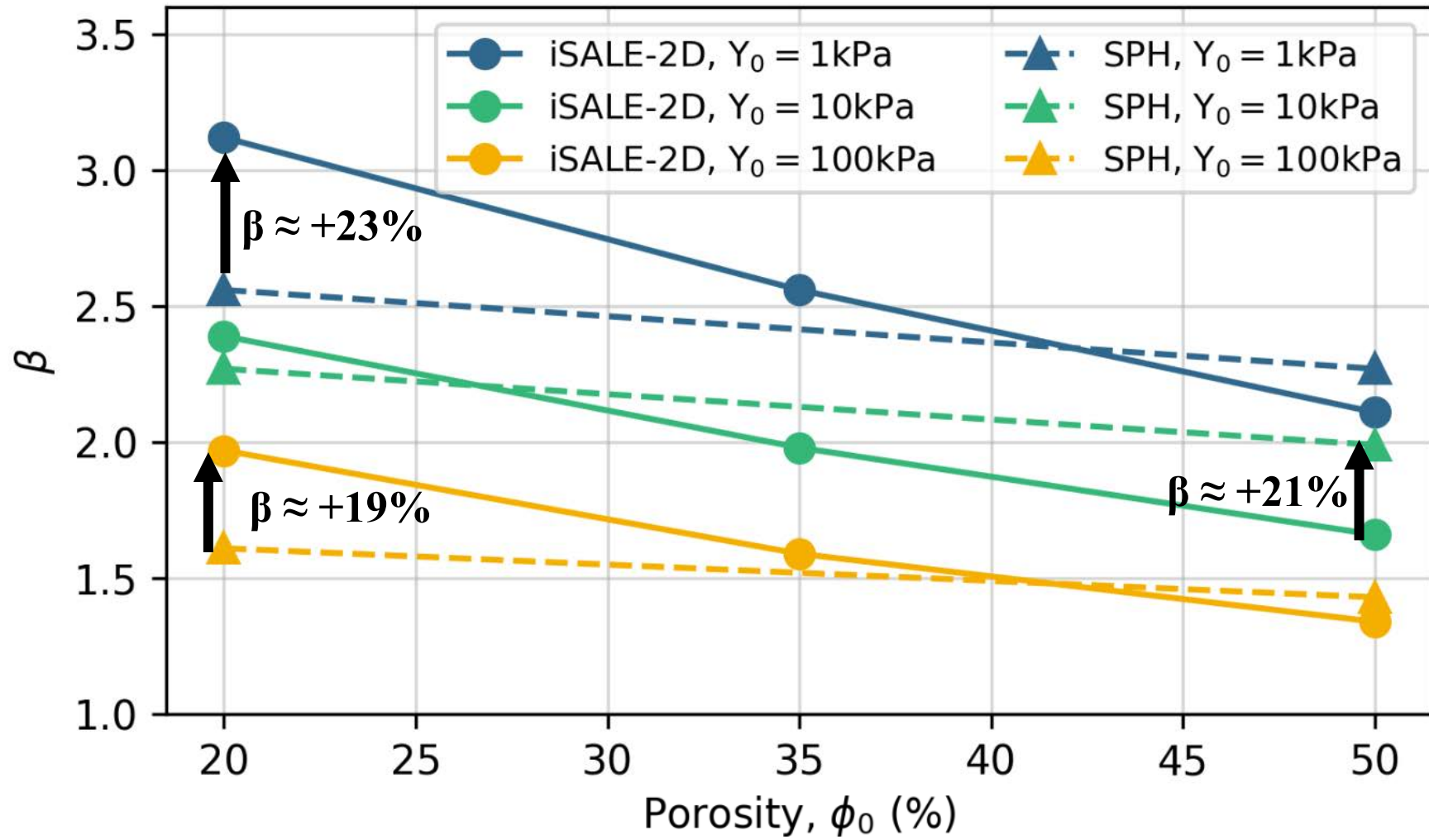
Strength model	Lundborg, $Y_0=1.4$ kPa, $f=0.77$
Porosity model $\Phi=42\%$	ϵ - α -model (iSALE), $\kappa=0.96$ P- α -model (SPH), $P_e=100$ Pa, $P_s=1.5$ GPa



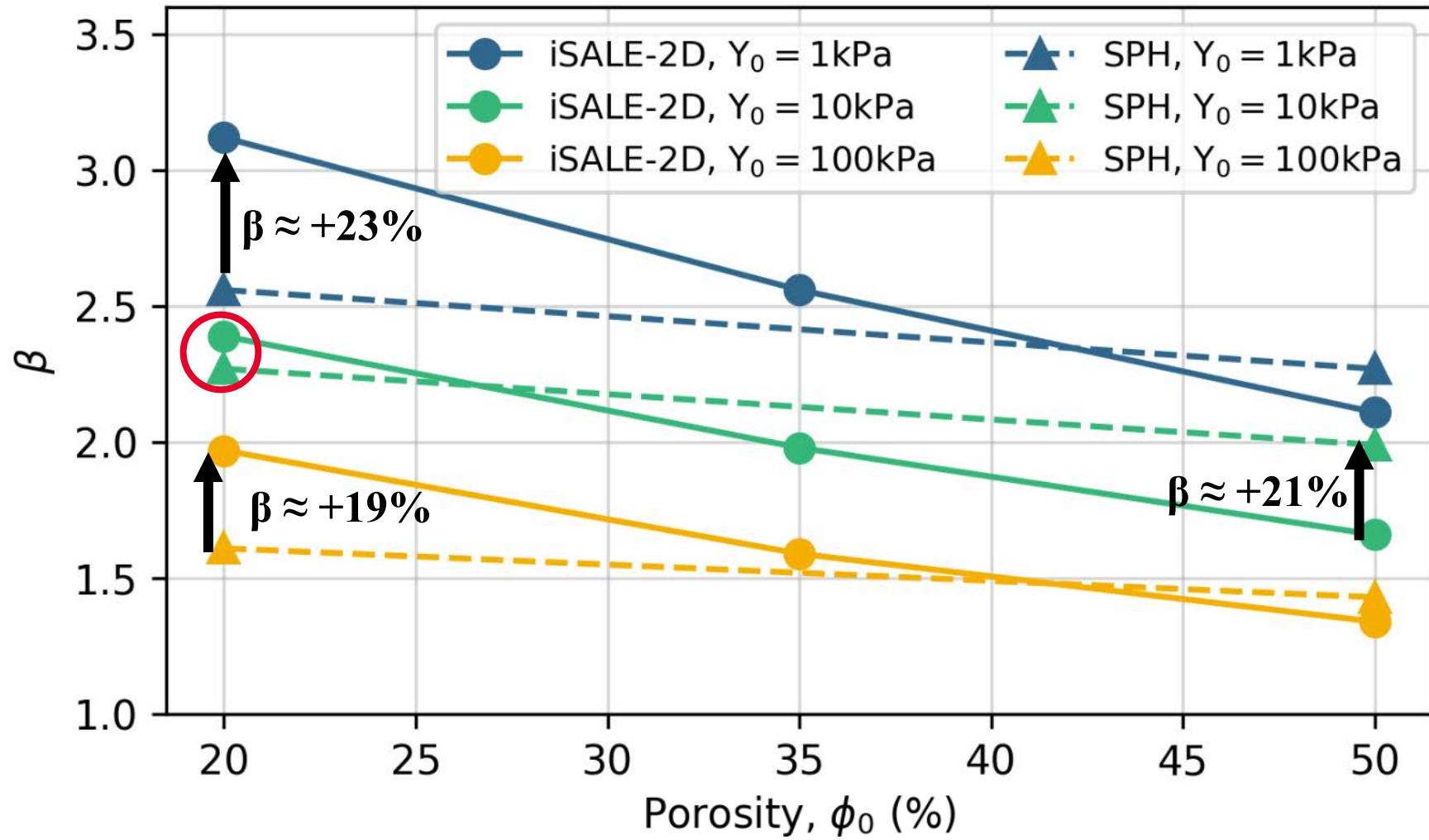
- Similar material models for iSALE-2D and SPH
- results from both codes agree with each other for a range of material parameters
- some deviations occur for small porosities ($Y_0=1$ kPa & 100 kPa) and at 50% ($Y_0=10$ kPa)



- Similar material models for iSALE-2D and SPH
- results from both codes agree with each other for a range of material parameters
- some deviations occur for small porosities ($Y_0=1$ kPa & 100 kPa) and at 50% ($Y_0=10$ kPa)

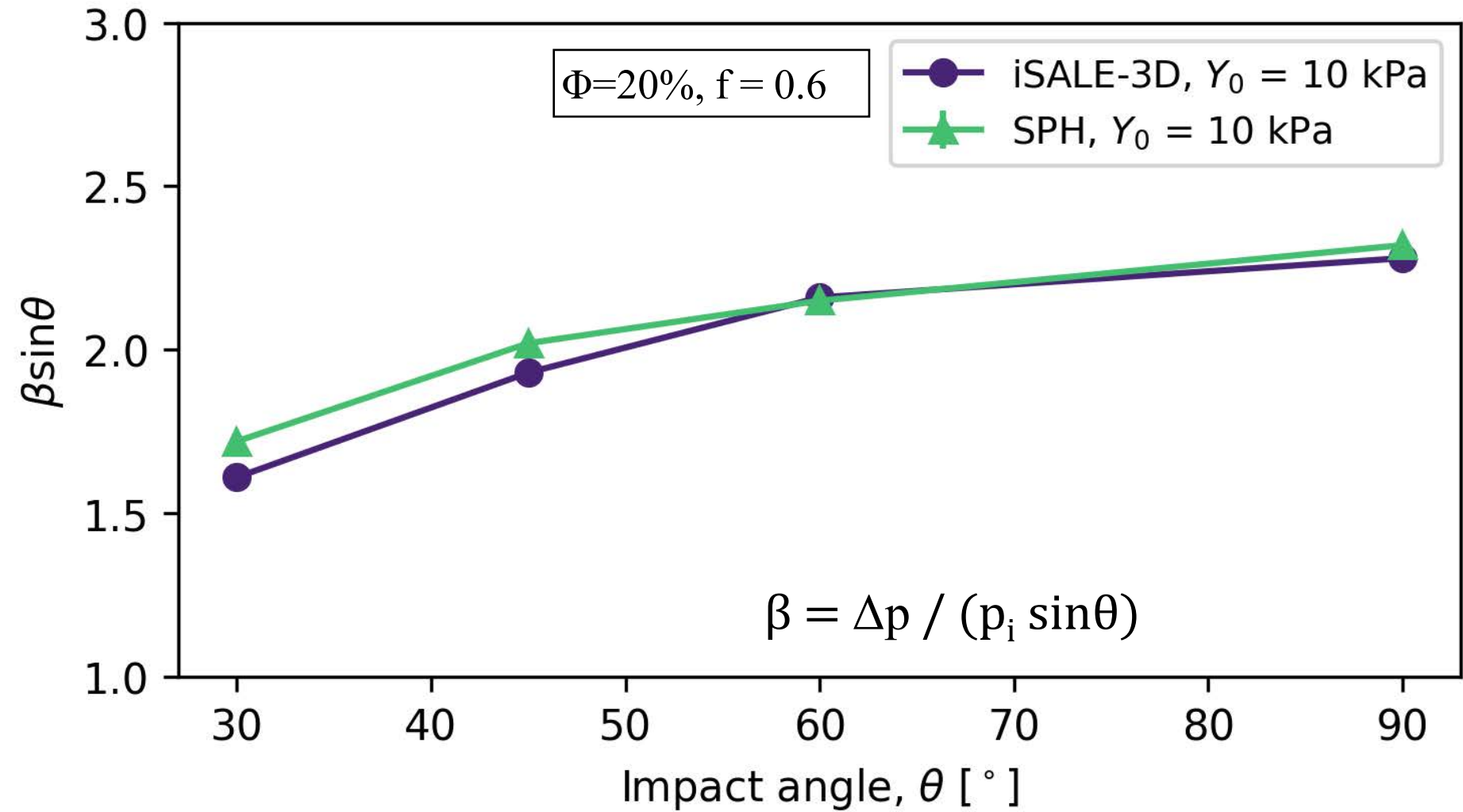


- Similar material models for iSALE-2D and SPH
- results from both codes agree with each other for a range of material parameters
- some deviations occur for small porosities ($Y_0=1$ kPa & 100 kPa) and at 50% ($Y_0=10$ kPa)

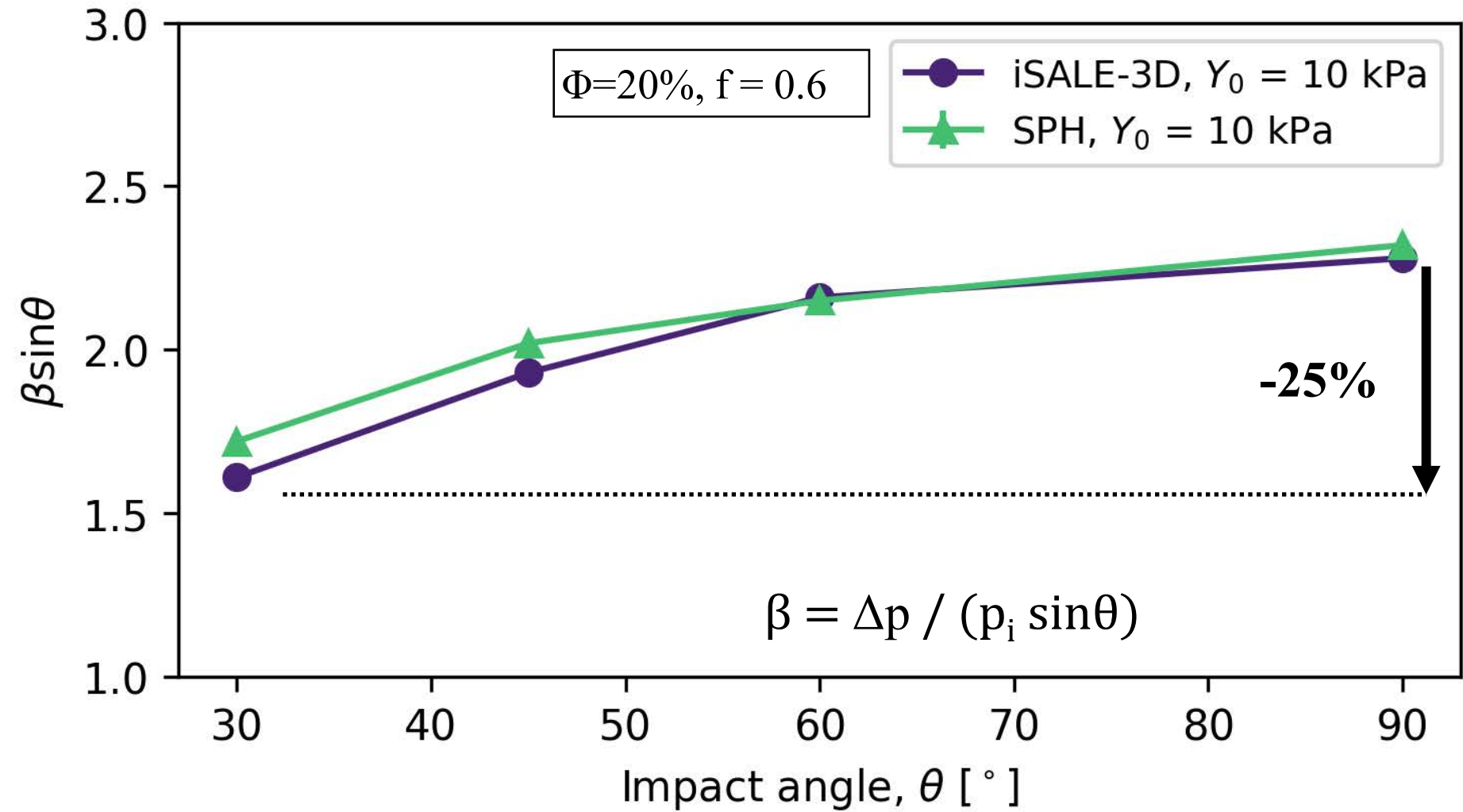


- Similar material models for iSALE-2D and SPH
- results from both codes agree with each other for a range of material parameters
- some deviations occur for small porosities ($Y_0=1$ kPa & 100 kPa) and at 50% ($Y_0=10$ kPa)

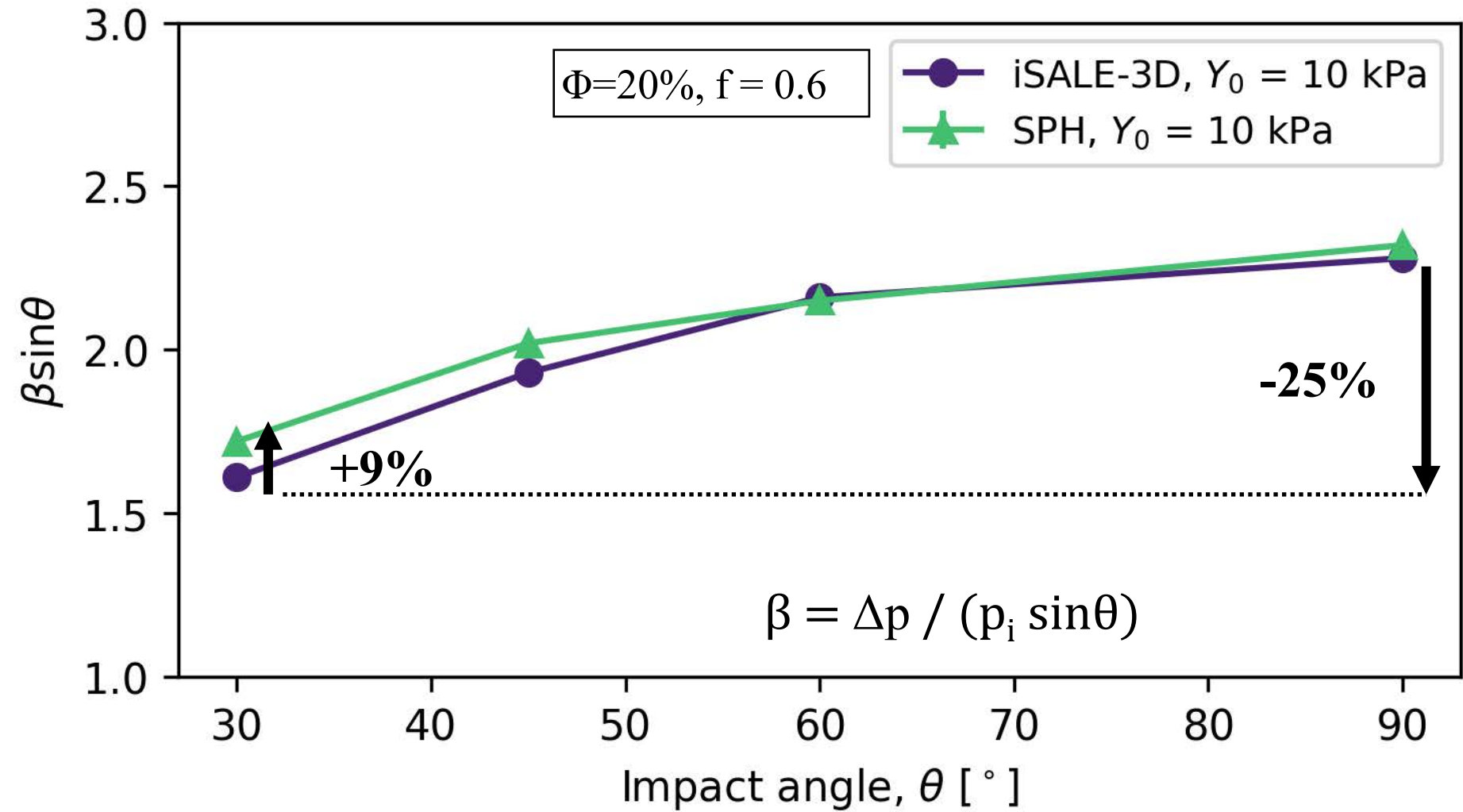
Effect of impact angle?



- same material models & parameters for iSALE-3D and SPH
- results from both codes agree with each other for all impact angles



- same material models & parameters for iSALE-3D and SPH
- results from both codes agree with each other for all impact angles



- same material models & parameters for iSALE-3D and SPH
- results from both codes agree with each other for all impact angles

Conclusion

Thank you.

- We have run **validation** tests in the Hera-relevant low strength regime for iSALE & SPH against experimental results for regolith simulant, **including measured values of β**
 → **both codes agree** with independent experimental data in terms of diameter, ejection behaviour and momentum enhancement
- Expanding the **benchmark to further materials** ($Y_0=1, 10, 100$ kPa, $\Phi=20-50\%$) shows **good agreement** between the codes ($<23\%$ deviation in β , in agreement to Stickle et al. 2020)
- Deviations for the impact angle scaled momentum between both codes for different **impact angle** are below 9%
- We plan further validations with other materials



This project has received funding from the European Union's Horizon 2020 research and innovation programme under grant agreement No 870377.



Near Earth Object
Modelling And Payloads
for Protection

Thank you.



NASA/Double Asteroid Redirection Test: Orbital perturbation by the ejecta-collision driven reshaping of Didymos after the impact event

Ryota Nakano and Masatoshi Hirabayashi
STAR Lab, Auburn University



IAA Planetary Defense Conference
26 – 30 April 2021



Didymos is spinning at close to its spin limit.

- Didymos is a ~ 780 m dia. top-shaped asteroid, spinning at 2.26 hr.
- May be structurally sensitive to reshaping
 - Even small perturbations may trigger reshaping.
 - Ejecta cloud hitting on Didymos (delivers kinetic energy)
 - Seismic shaking attenuation due to the DART impact

Understanding the orbital perturbation due to reshaping is important to determine the momentum transfer coefficient and to assess the DART deflection capability.

Statistically determine the effect of asymmetric reshaping.

How Didymos' reshaping affects the orbital period after the DART impact?

- While the reshaping magnitude is unknown, we have knowledge of possible reshaping processes of top-shaped asteroids.
 - Ejecta will distribute heterogeneously on Didymos, which will lead to asymmetric reshaping.
- We developed a shape model generator to create “reshaped” shape models.

6,000 asymmetric reshaped cases are prepared.

- We characterize the reshaping with 4 parameters: α_{+x} , α_{-x} , α_{+y} , and α_{-y} .
- Each represents the ratio of the $\pm x$ or $\pm y$ axis for the reshaped body to that of the original body.
- We randomly define a value for each, in a range from 1 to α_{max} . (= maximum reshaping magnitude).
- α for z axis is uniquely determined by keeping the volume constant regardless of the shape.

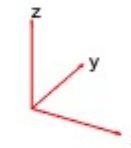
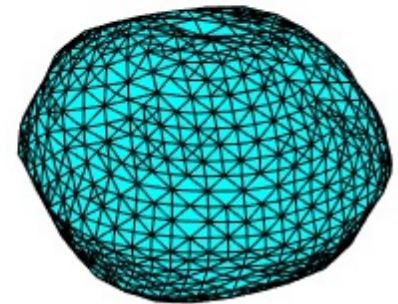
Ex: $\alpha_{max} = 1.1 \approx 40 m$

$$\alpha_{+x} = 1.099 \approx 38 m$$

$$\alpha_{-x} = 1.085 \approx 33 m$$

$$\alpha_{+y} = 1.021 \approx 8 m$$

$$\alpha_{-y} = 1.049 \approx 19 m$$



12 different α_{max} ,

500 cases for each α_{max}

→ 6,000 simulation cases in total

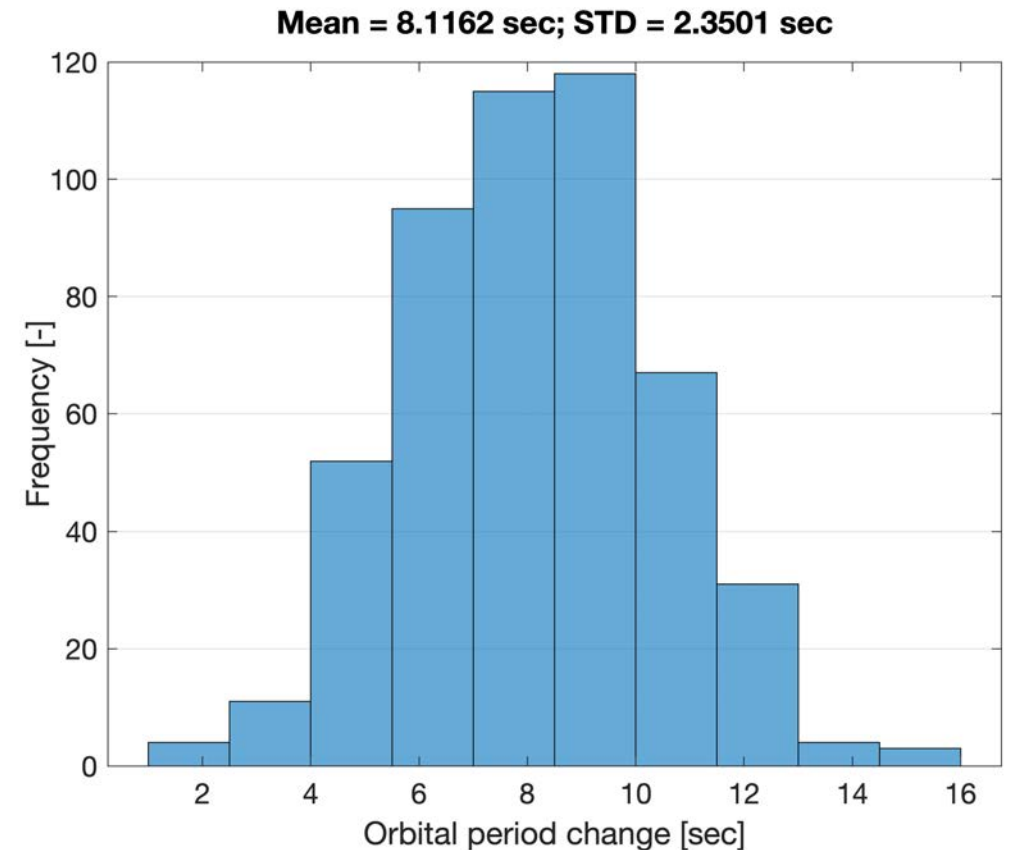
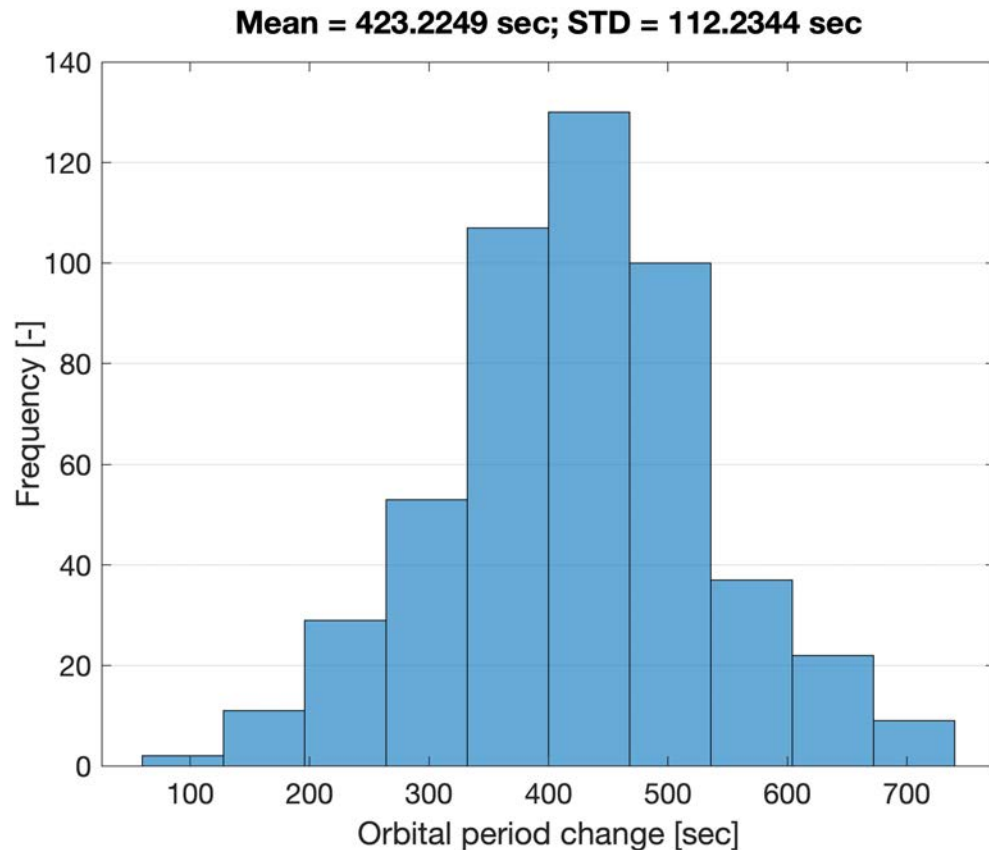
Dimorphos' orbital period change after 180 days from the impact

$$\alpha_{max} = 1.05$$

→ less than 20 m of reshaping

$$\alpha_{max} = 1.001$$

→ less than 1 m of reshaping

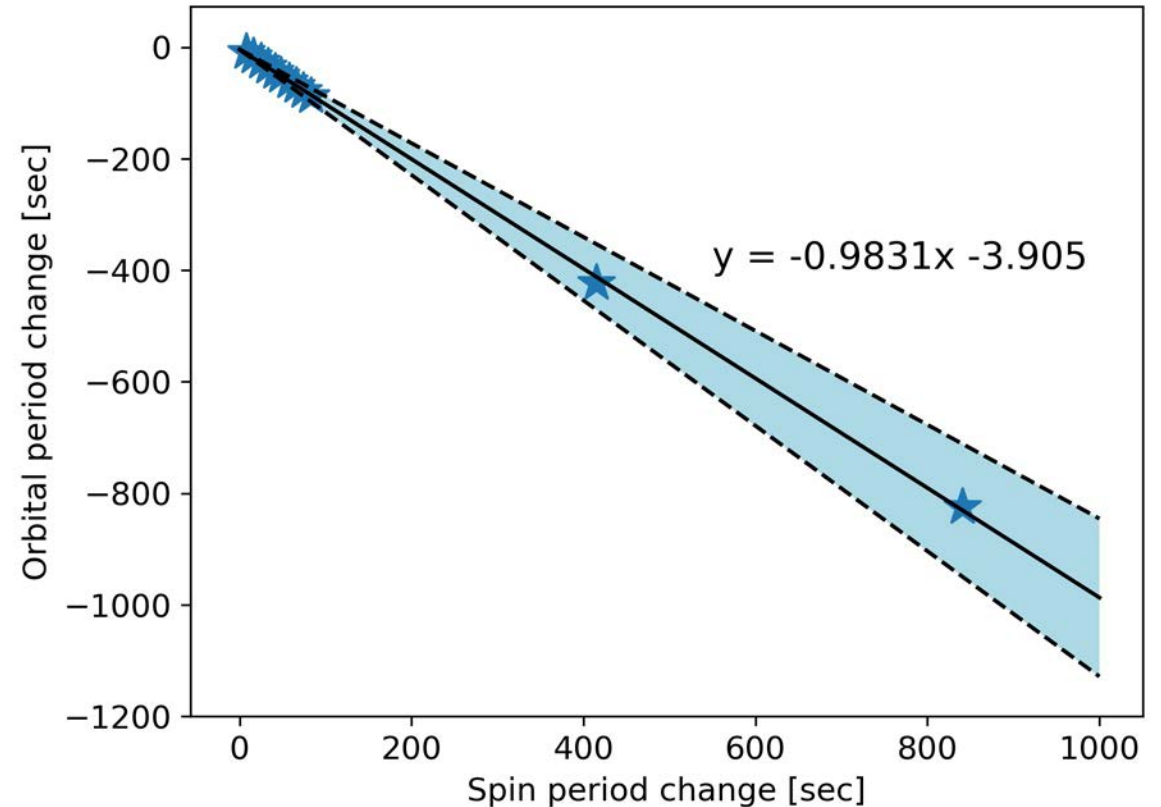


Reshaping magnitude can be constrained with the spin period change.

Didymos' angular momentum should be conserved.

→ The spin period changes during the reshaping event.

α_{max}	(Reshaping scale)	$\Delta\bar{P}_{spin}$ [sec]
1.1	(≈ 40 m)	840.57
1.05	(≈ 20 m)	415.09
1.01	(≈ 4 m)	82.684
1.009	(≈ 3.5 m)	74.192
⋮		⋮
1.002	(≈ 0.8 m)	15.701
1.001	(≈ 0.4 m)	8.0486



The orbital period linearly decreases as reshaping mag. increases.

From the statistical investigation, we found:

- For a shape change of less than 40 m, the reshaping-driven orbital period change is characterized to be linear.
- We predict the relationship: $\Delta P_{orb} = -0.9831 \Delta P_{spin} - 3.905$
- The orbital period should always become shorter than the original period, for the head-on DART impact scenario.
- Detailed observation of Didymos' spin period change can constrain the magnitude of reshaping,
- from which we can decouple the reshaping-driven orbital period change and can accurately determine the momentum transfer efficiency.

Thank you!



IAA Planetary Defense Conference
26 – 30 April 2021



12 different α_{max} , 500 cases for each α_{max} , 6,000 simulation sets

α_{max}	$\Delta\bar{P}_{spin}$	$\Delta\bar{P}_{orb}$
1.1	840.57	824.47
1.05	415.09	423.22
1.01	82.684	87.354
1.009	74.192	78.527
1.008	65.933	69.719
1.007	57.823	61.155
1.006	47.863	51.004
1.005	40.937	43.781

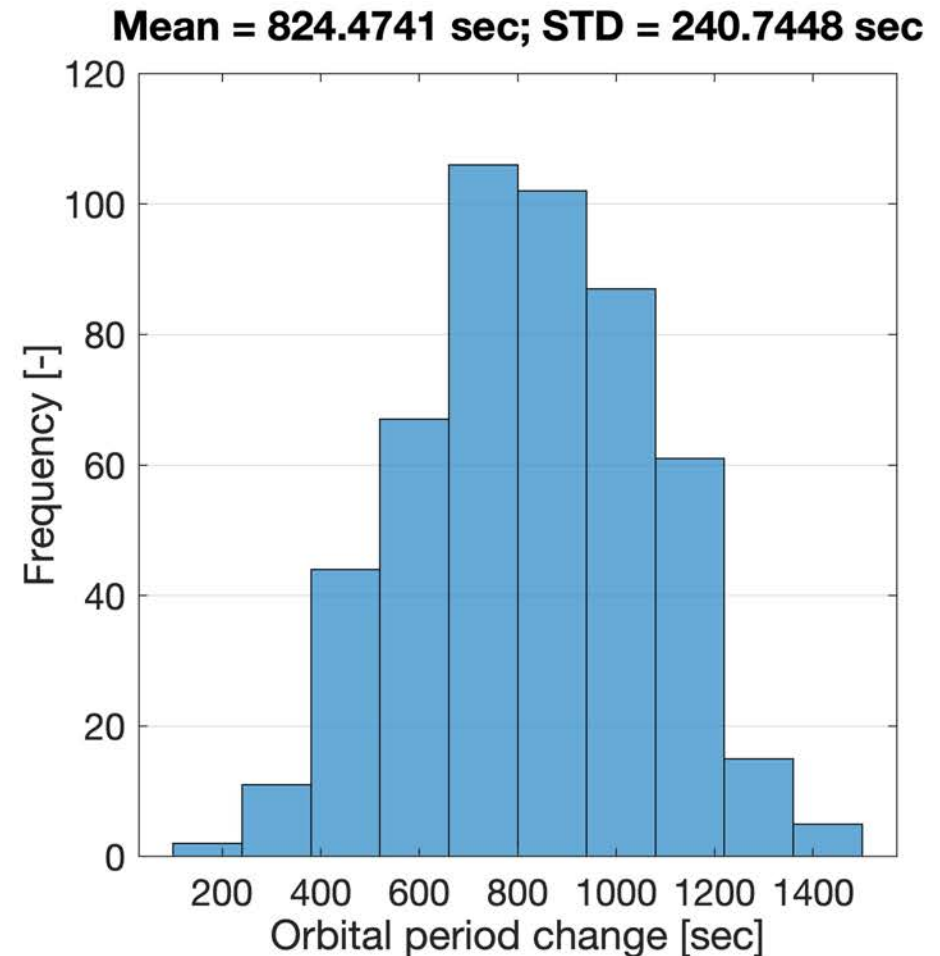
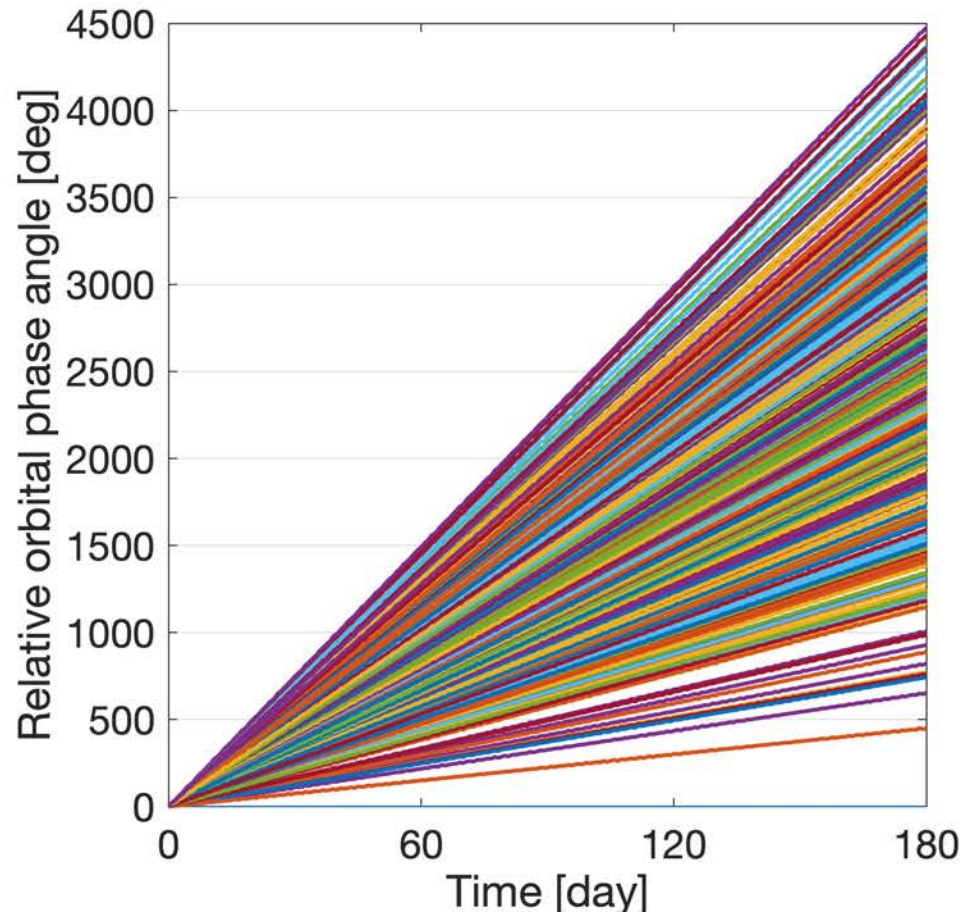
α_{max}	$\Delta\bar{P}_{spin}$	$\Delta\bar{P}_{orb}$
1.004	32.844	34.983
1.003	24.762	26.054
1.002	15.701	16.078
1.001	8.0486	8.1162

$\Delta\bar{P}_{spin}$: Mean spin period change

$\Delta\bar{P}_{orb}$: Mean orbital period change

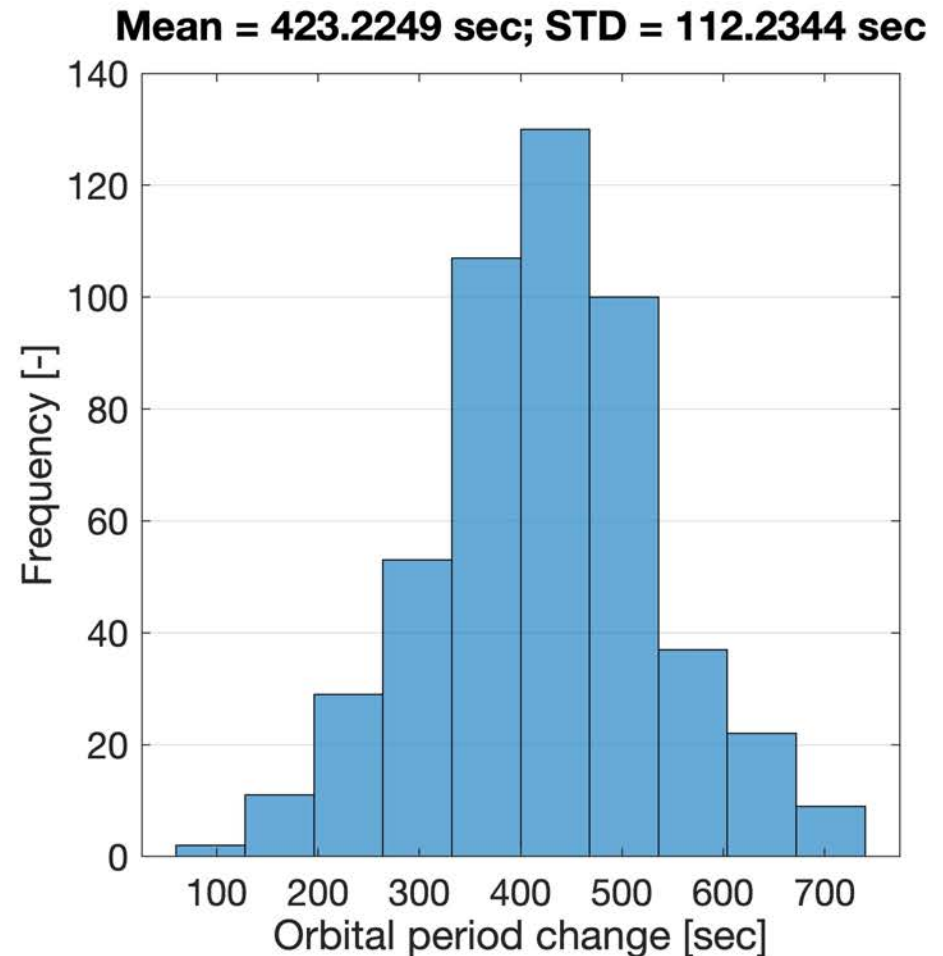
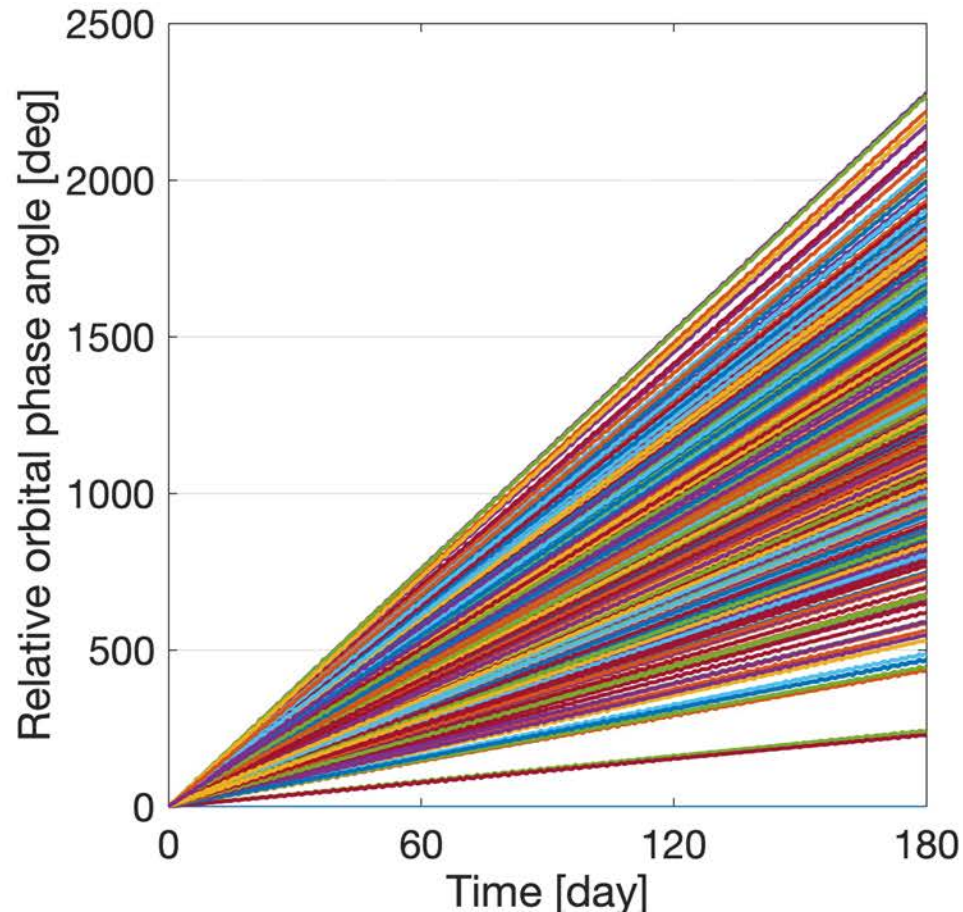
Relative phase angle evolution 180 days after the DART impact

$\alpha_{max} = 1.1 \rightarrow$ less than 40 m of reshaping in each axis



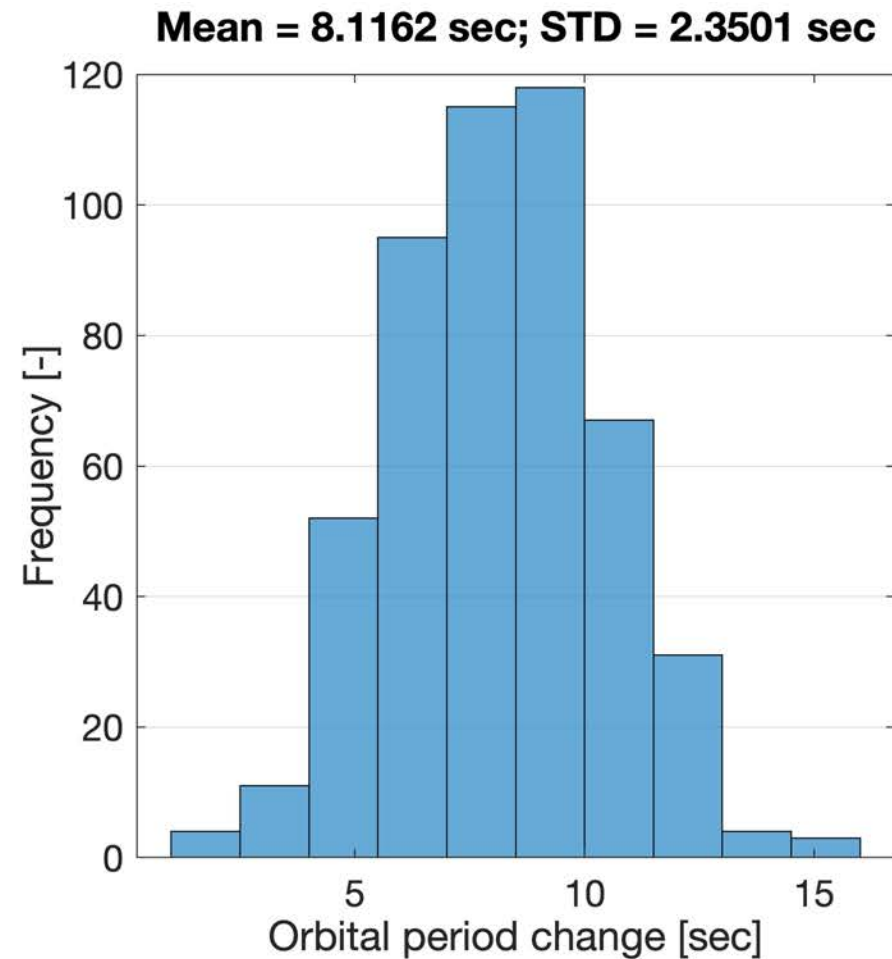
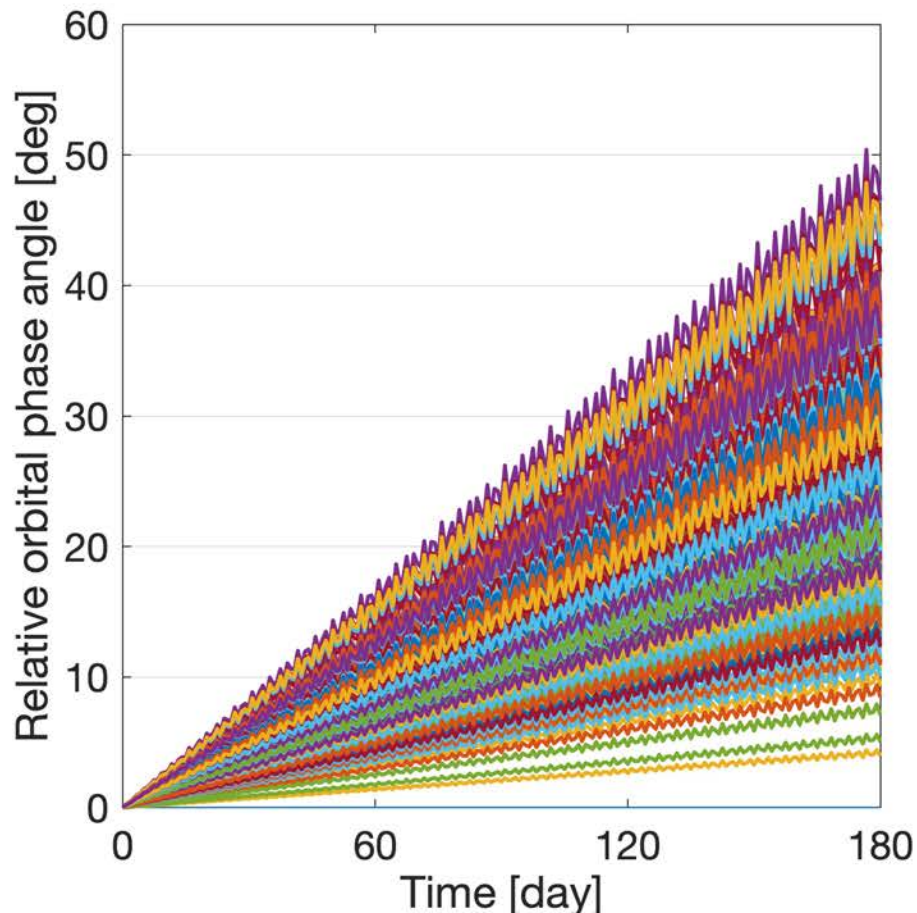
Relative phase angle evolution 180 days after the DART impact

$\alpha_{max} = 1.05 \rightarrow$ less than 20 m of reshaping in each axis



Relative phase angle evolution 180 days after the DART impact

$\alpha_{max} = 1.001 \rightarrow$ less than 1 m of reshaping in each axis



Late-time Nuclear Disruption in the PDC 2021 Scenario

Patrick King¹, Megan Bruck Syal², David S.P. Dearborn², Robert Managan², J. Michael Owen², and Cody Raskin²

Session 7a: Deflection & Disruption Modeling and Testing

Paper 151

04/28/21

¹Johns Hopkins University Applied Physics Laboratory
Space Exploration Sector
11100 Johns Hopkins Road
Laurel, MD 20723

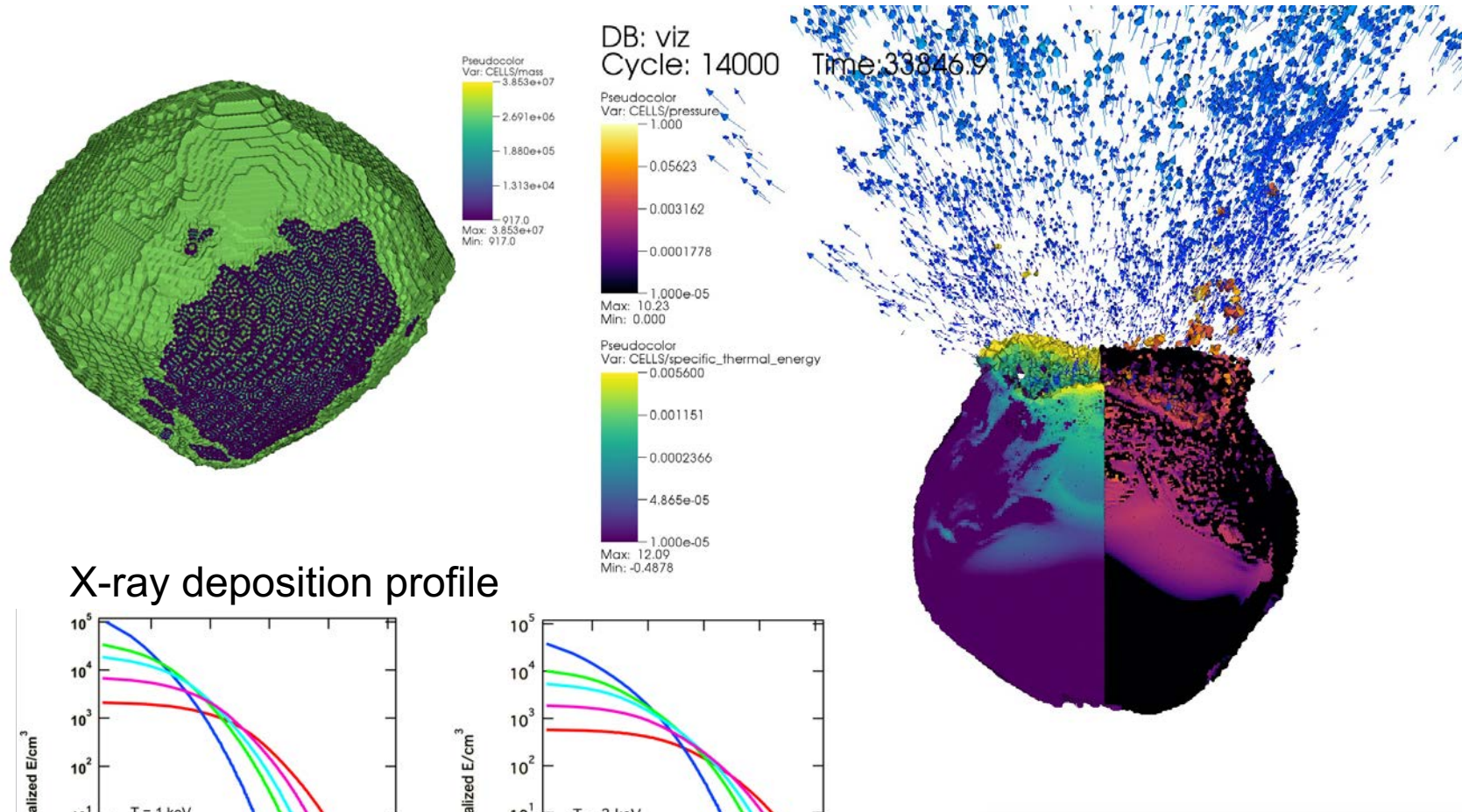
²Lawrence Livermore National Laboratory
7000 East Avenue
Livermore, CA 94550

Overview

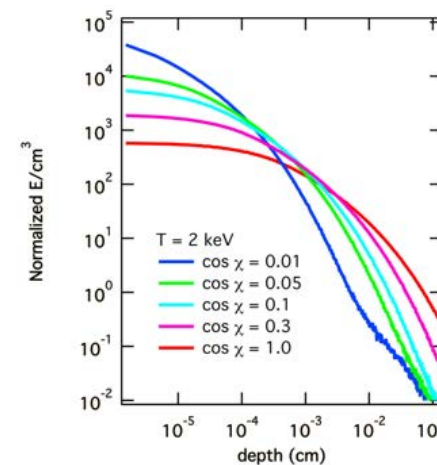
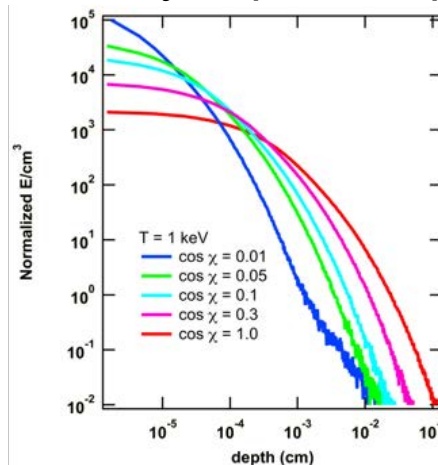
- Nuclear Disruption of a Fiducial Small Body
- N-Body Methodology
- Results for the PDC 2021 Scenario

Nuclear Disruption of a Fiducial Small Body

- Simulation conducted with Spherical hydrocode
- 20% scaled model of 101255 Bennu (corresponds to 100 meter diameter)
- Modeled as uniform granite with 25% microporosity; Collins strength model with Tillotson EOS
- Uniform bulk linear resolution (~1.6 meter linear resolution) with ratioed zoning deposition zone for source
- 1 MT device at 15 meter height-of-burst (65 meters from center) at equator
- Consistent with simulation scheme described in Dearborn et al. 2020

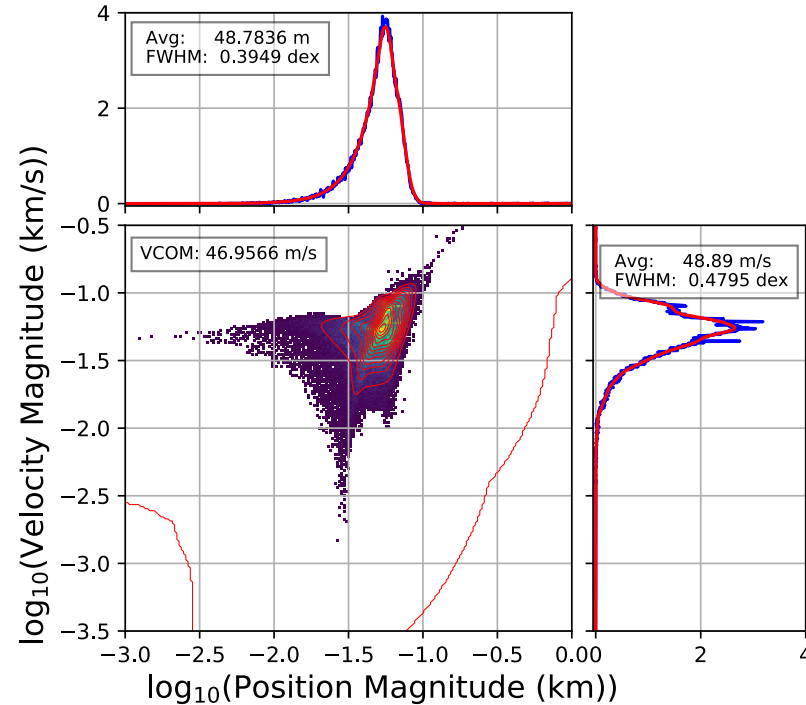


X-ray deposition profile

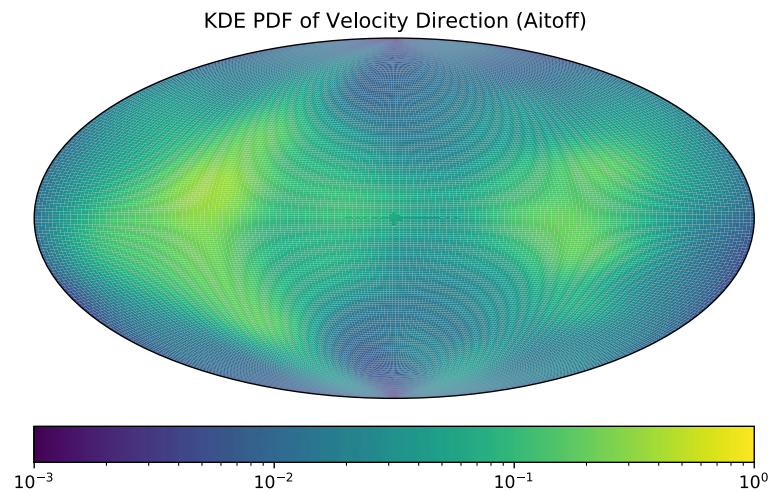
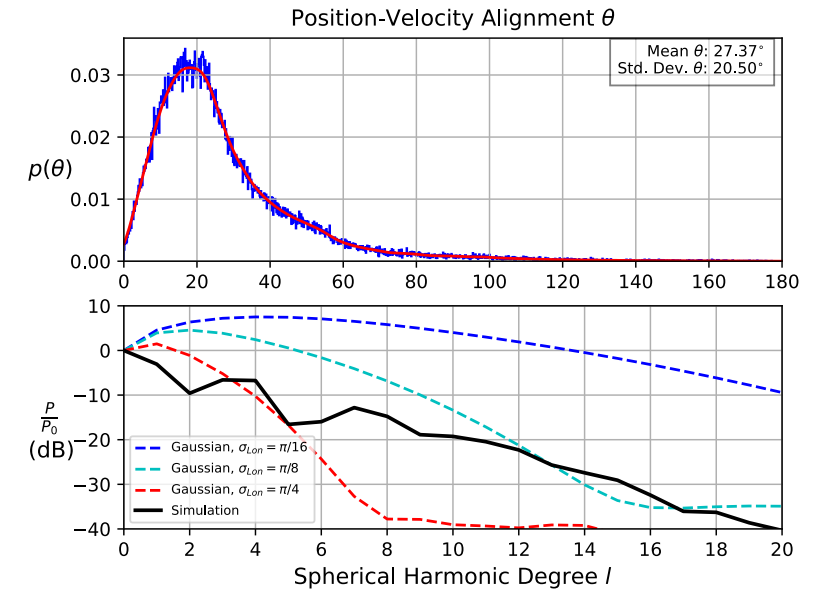


Nuclear Disruption of a Fiducial Small Body

- Simplified treatment of fragmentation: using bulk particles as estimate of disrupted debris field
- Delivered about 60 kT of yield to the target; about 4 kT of this was debris field kinetic energy (~0.35% KE yield efficiency)
- Kinetic Energy/Mass of ~17000 J/kg (much greater than Q^*_D)
- Center of mass velocity (a deflection) of 46.96 m/s
- COM frame expansion velocity (disruption) of 48.89 m/s
- Expansion field in COM frame is nearly uniform and radial
- Details to appear in King et al., submitted to Acta Astronautica

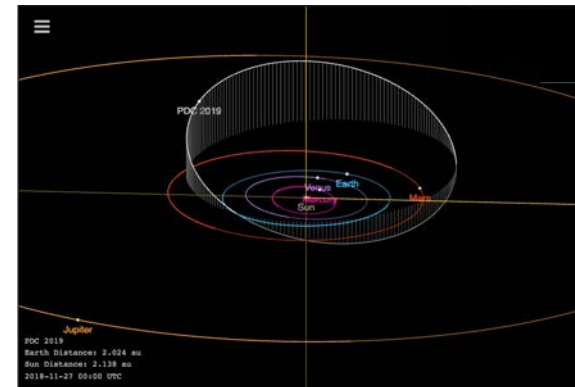
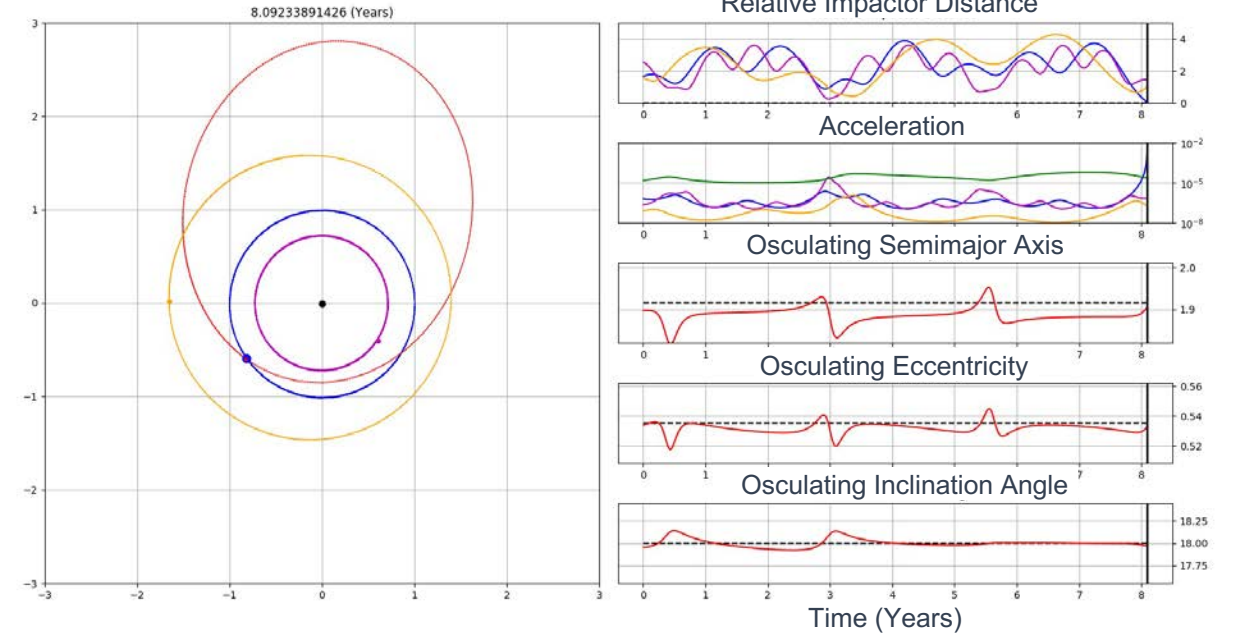


Calculated Deflection: 46.96 m/s
 Calculated Disruption: 48.89 m/s

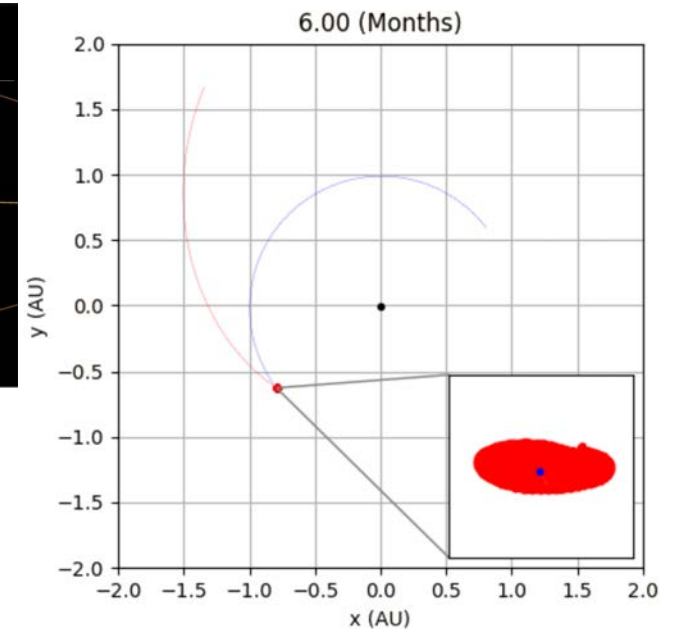


N-Body Methodology

- Approach is to insert an approximate fragment field directly into a realistic N-body model of the solar system and evolve fragment orbits
- Fragment field based on disruption simulation and consists of deflection and disruption components
- Softening is employed to ensure stability and speed; carefully controlled for accuracy bounds
- Care is taken to ensure the initial trajectory results in an impact
- Effects such as gravitational focusing included to orbital evolution accuracy
- Fragment-fragment gravity is included



Example based on the 2019 PDC Scenario

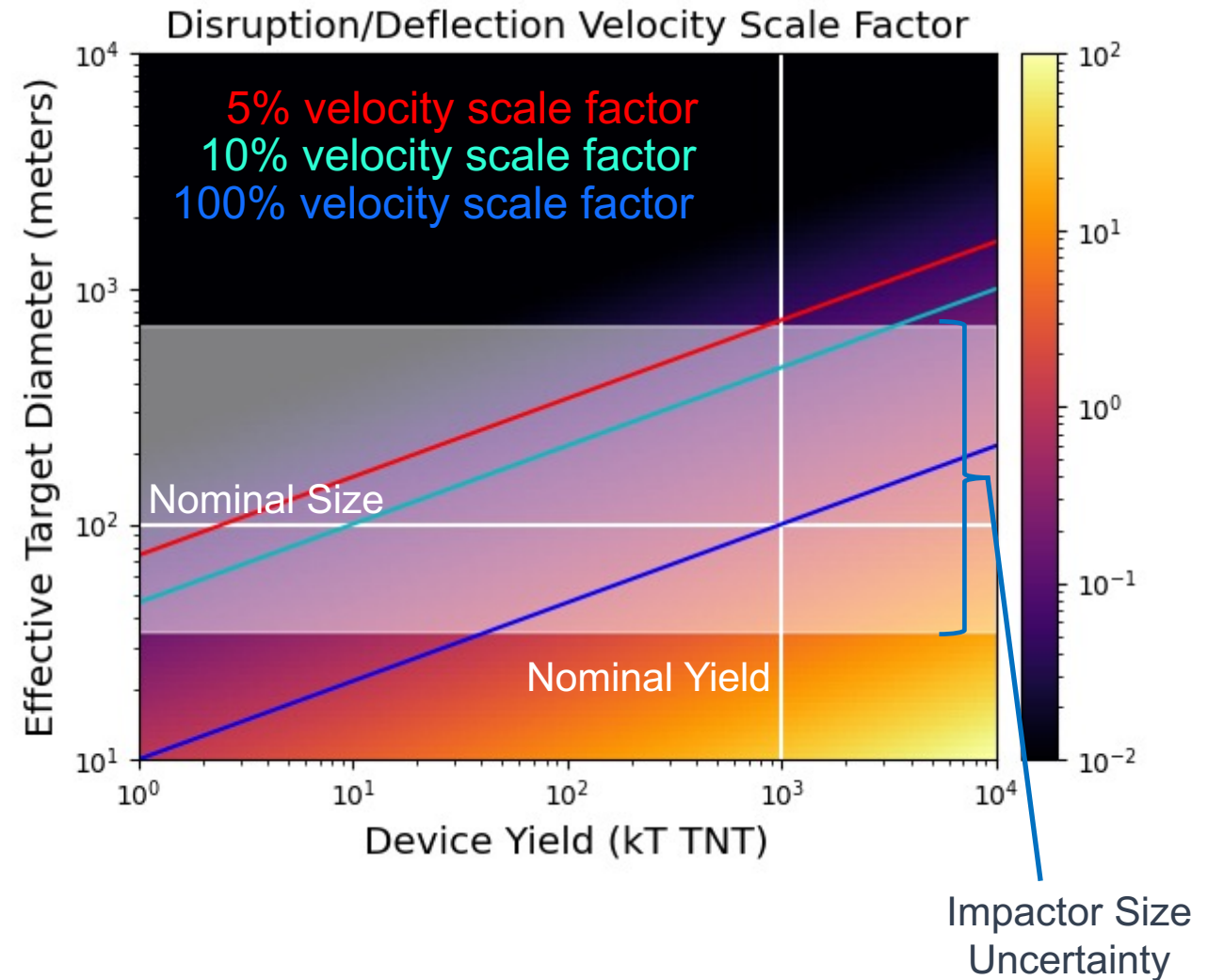


N-Body Methodology

- Can apply a naïve yield scaling to accommodate either different yields or uncertainty in target size

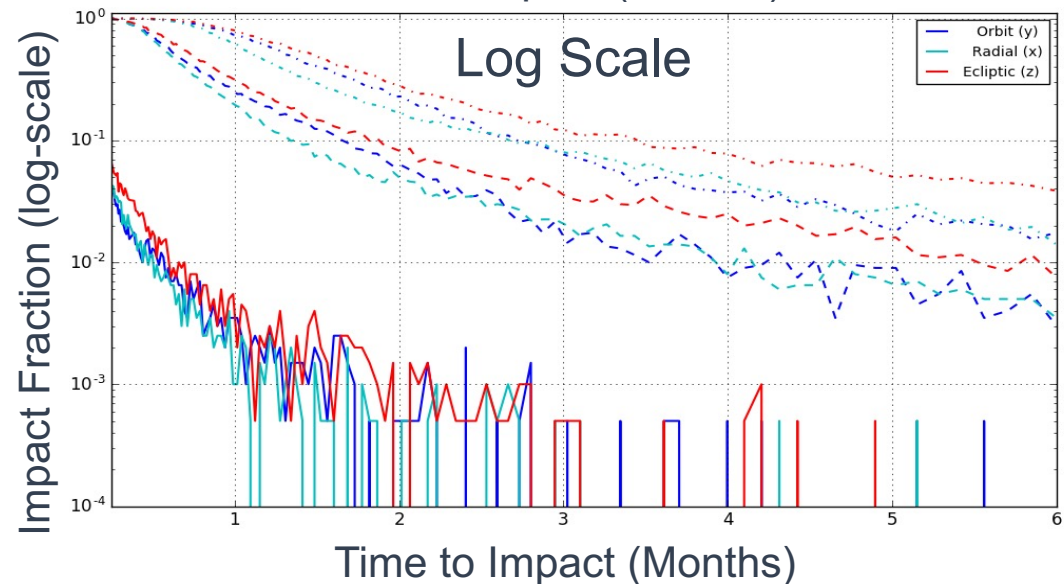
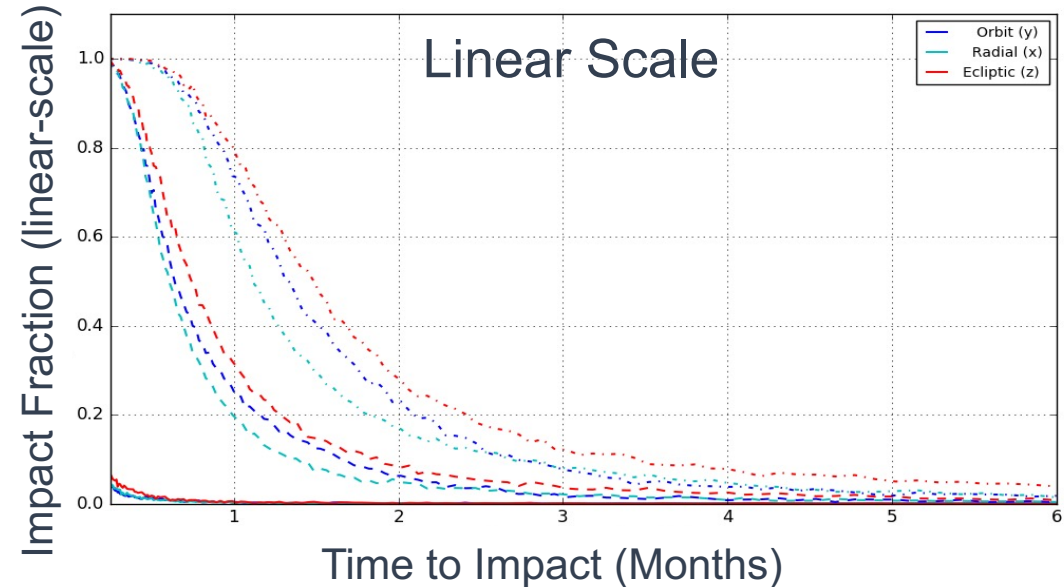
$$\frac{v_{scaled}}{v_{nominal}} = \left(\frac{Y}{1 \text{ MT TNT}} \right)^{1/2} \left(\frac{D}{100 \text{ m}} \right)^{-3/2}$$

- Study should be repeated with dedicated high-fidelity disruption simulation using best available target data
- Primary metric is the *impact fraction* (quantity of impacting mass relative to total mass)
- This study has been conducted for the PDC 2019 scenario and several other reasonable scenarios and is to appear in King et al., submitted to Acta Astronautica



Results for the PDC 2021 Scenario

- The nominal disruption model can disrupt the impactor efficiently enough to result in only 1% impacting mass by two weeks
 - By 2 months the nominal disruption has likely achieved 0.1% impact fraction, but this estimate is limited by the fragment resolution of our simulations
- The less efficient disruptions require more time before impact to work effectively
 - The 10% scaled disruption achieves impact fraction of 10% by 2 months; 5% scaled disruption requires 3.5 months
- Deflection direction appears to have a modest effect; the strongest performing direction is the radial direction and the weakest is the ecliptic direction





JOHNS HOPKINS
APPLIED PHYSICS LABORATORY

An Overview of Numerical Radiation Transport Techniques in Asteroid Deflection Modeling

Planetary Defense Conference 2021

April 28, 2021
Vienna, Austria

Nicholas A. Gentile

 Lawrence Livermore
National Laboratory

P. O. Box 808, Livermore, CA 94551

LLNL-PRES-821466

This work was performed under the auspices of the U.S. Department of Energy by Lawrence Livermore National Laboratory under Contract DE-AC52-07NA27344. Lawrence Livermore National Security, LLC.



Photon transport is necessary to accurately model deflection scenarios using x-ray deposition

- Inertial confinement fusion (ICF) and asteroid simulations share some commonalities and challenges
 - Both have large length, density, and opacity scales
- ICF codes discretize in space and time
 - Zones have ρ , T , P , radiation intensity, etc.
 - Energy deposition done by a radiation transport method
 - Hydrodynamic motion and shocks handled by a hydro method
 - Radiation and matter are coupled by thermal emission from material and electron and ion conduction
- Transport dominates the simulation run time
 - We face tradeoffs in the radiation methods between speed and accuracy

- Both model round things suspended in vacuum hit by x-rays
- We can use the same code for both

The transport equation describes the motion of photons including interactions with moving matter

Photons move in straight lines at speed c

In-scattering

Out-scattering

Absorption (Doppler-shifted)

Thermal emission Doppler-shifted

Stimulated scattering

$$\frac{1}{c} \frac{\partial I(\nu, \Omega)}{\partial t} + \Omega \cdot \nabla I(\nu, \Omega) = -\gamma D \sigma_a I(\nu, \Omega) + \sigma_a \frac{B[\nu, T]}{[\gamma D(\Omega)]^2} + \int_0^\infty d\nu' \int_{4\pi} d\Omega' \frac{\nu}{\nu'} \sigma_s(\nu' \rightarrow \nu, \Omega' \rightarrow \Omega) I(\nu', \Omega') \left[1 + \frac{c^2 I(\nu, \Omega)}{2h\nu^3} \right] - \int_0^\infty d\nu' \int_{4\pi} d\Omega' \sigma_s(\nu \rightarrow \nu', \Omega \rightarrow \Omega') I(\nu, \Omega) \left[1 + \frac{c^2 I(\nu', \Omega')}{2h\nu'^3} \right]$$

with $\gamma \equiv \left(1 - \frac{v^2}{c^2}\right)^{-\frac{1}{2}}$ and $D \equiv 1 - \Omega \cdot \frac{v}{c}$ arising from material motion and $B(\nu, T) = \frac{2h\nu^3}{c^2} \left[\exp\left(\frac{h\nu}{kT}\right) - 1 \right]^{-1}$ the Planck function describing thermal emission in Local Thermodynamic Equilibrium

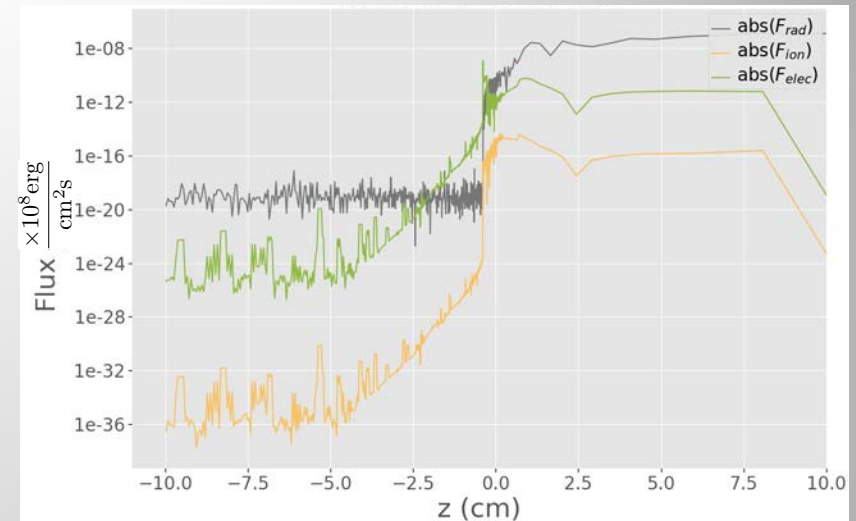
- This is the Boltzmann equation written in terms of Intensity
 - I has units of Energy/(Length²-Time-Steradian)
- Material motion corrections (MMC) need to be included
 - Emission isn't isotropic, absorption is angle dependent
 - There are many $O(v/c)$ MMC approximations; also many numerical simplifications are employed, some inaccurate
- Radiation exchanges energy and momentum with matter

The two common numerical methods for transport simulations are IMC and S_N

- Implicit Monte Carlo (IMC) simulates radiation by computational particles with randomly selected emission positions and directions
 - Emit, scatter, track, and absorb “fake” photons
 - “implicit” refers to a numerical extrapolation in time of the matter temperature used in emission
 - Allows accurate simulation of scattering and Doppler shifts
 - Energy-angle correlation in Compton scattering can be simulated
 - Use of random numbers causes statistical noise $\sim N_{\text{particles}}^{-1/2}$ in the results
 - Reducing the slowly-declining noise leads to long simulation times
 - Discretization errors in thermal emission, both temperature and emission location, require small Δx and Δt
 - Stimulated Compton is approximated or ignored
- S_N or Discrete Ordinates represents I at fixed angles using finite element basis functions in each zone
 - The discrete angles are selected to enable Gauss integration of spherical harmonics
 - Faster than IMC (>10x in opaque problems)
 - Fully implicit in emission temperature; smaller spatial discretization error
 - Can simulate stimulated Compton
 - The use of discrete angles makes anisotropic scattering approximate and can lead to simulation artifacts

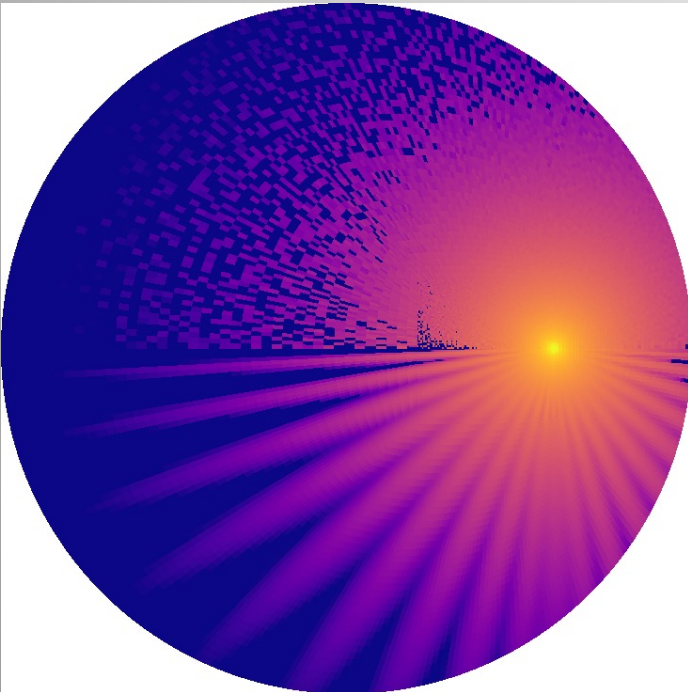
Computational artifacts of IMC and S_N

- IMC simulation of radiation flux in an illuminated asteroid shows statistical noise
- The electron and ion conduction flux also shows noise, seeded by the IMC through its effect on the electron temperature



Simulation with an isotropic point source in an absorbing non-scattering medium

- IMC simulation (top) shows statistical noise
- S_N simulation shows ray effects



Flux-limited Diffusion is a quick but very approximate transport simulation technique

- Averaging the transport equation over angle plus an ansatz for the flux results in diffusion equation

$$\frac{\partial E}{\partial t} + \nabla \cdot [-\mathcal{L}F] + \frac{4}{3} \nabla \cdot (Ev) + \frac{1}{3} v \cdot \nabla E = c\sigma_a T^4 - c\sigma_a E$$

Here $E = -\frac{1}{c} \int_{4\pi} d\Omega I$ is the radiation energy density (Energy/Length³) and

Material motion correction terms

$$F = -\frac{c}{3(\sigma_a + \sigma_s)} \nabla E$$

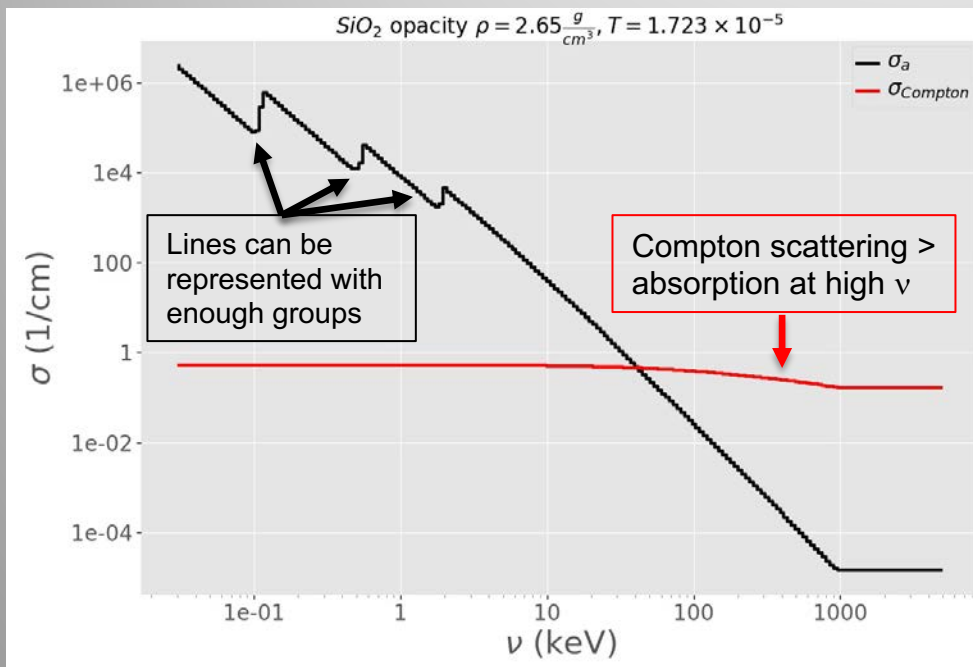
is the radiation flux (Energy/Length²-Time)

- This expression for F is an approximation

- Diffusion can't model angular information – no shadows
- Diffusion is accurate when radiation is isotropic AND gradients in E are small
 - Ad hoc flux limiter \mathcal{L} in $[0, 1]$ needed to suppress superluminal energy flow ($F > c \Delta E$) when σ is small
- For heat conduction in electrons and ions, which typically have small flux, a similar diffusion approximation is accurate

The Multigroup approximation is used to express frequency dependence of σ and I (or E)

- We pick $O(10)$ -(100) fixed values of ν ; each range is called a “group”
 - Group bounds are constant in time and space in a simulation
 - We solve one transport or diffusion equation per group
 - Scattering and absorption-reemission couple the groups and the per-group equations
 - This requires iteration in S_N and FLD



- Opacities are constant in each group during a time step
 - Recalculated in each group at the beginning of the time step to account for changes in ρ and T

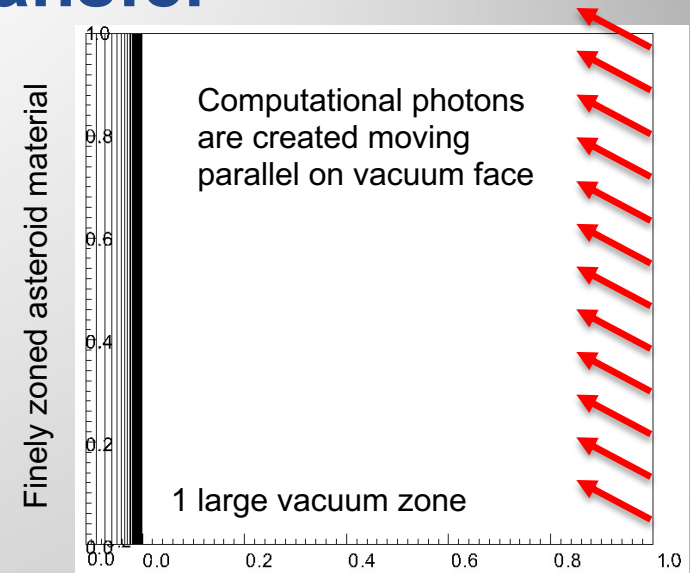
We are using IMC in our deflection calculations because they contain vacuum and point sources

- Diffusion has poor accuracy in vacuum
 - It also can't simulate the directionality of a point source
- S_N suffers from ray effects in vacuum
 - Can't accurately model strongly peaked scattering like Compton
- IMC can simulate point and ray sources
 - We have to incur and mitigate the drawbacks:
 - Statistical noise
 - Long runtimes
 - Use lots of zones and time steps

We must use lots of particles and processors

1D simulations simulate surface absorption, reemission, and momentum transfer

- 1 sq. cm chunk ~ 60 cm deep
- Source equivalent to 1 kiloton 85 m away
 - Spectrum = 1 keV Planckian
- 200 groups in $[3 \times 10^{-3}, 1000]$ keV log-spaced
- Run to ~ $1e-4$ sec
 - Δt in $[10^{-16}, 10^{-9}]$ sec
- 2000 zones with Δx in $[10^{-5}, .4]$ cm
- 10^6 computational photons
- Materials = SiO₂, Fe, H₂O, Fosterite
- Simulations take ~ 1 Day on 144 2.1 MHz procs
- Hydrodynamics is Lagrangian
 - Mesh moves with the material

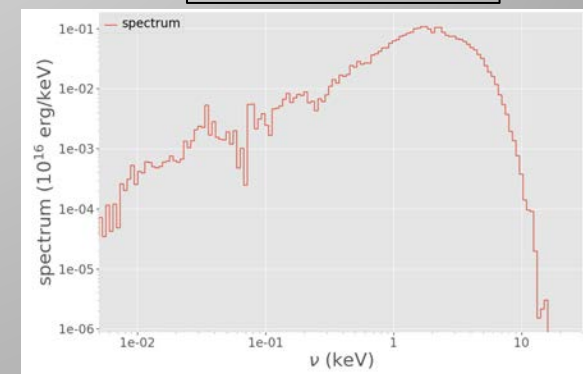
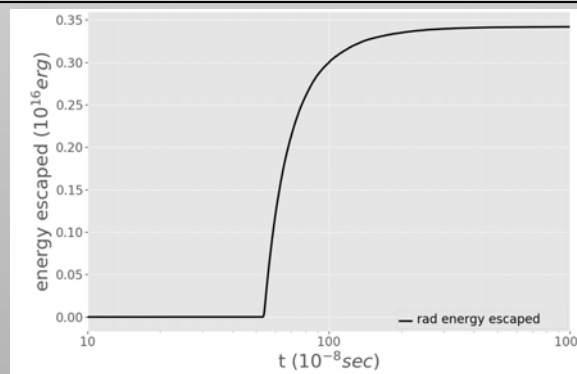
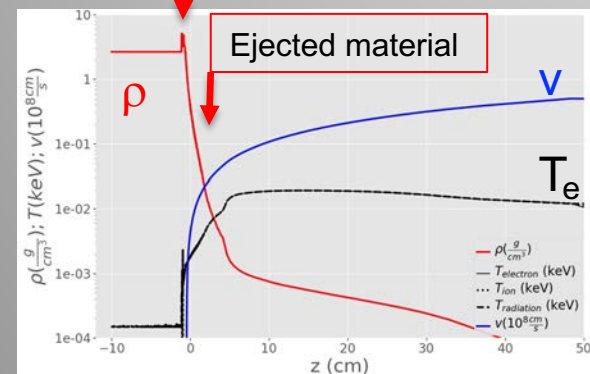


Ingoing shock

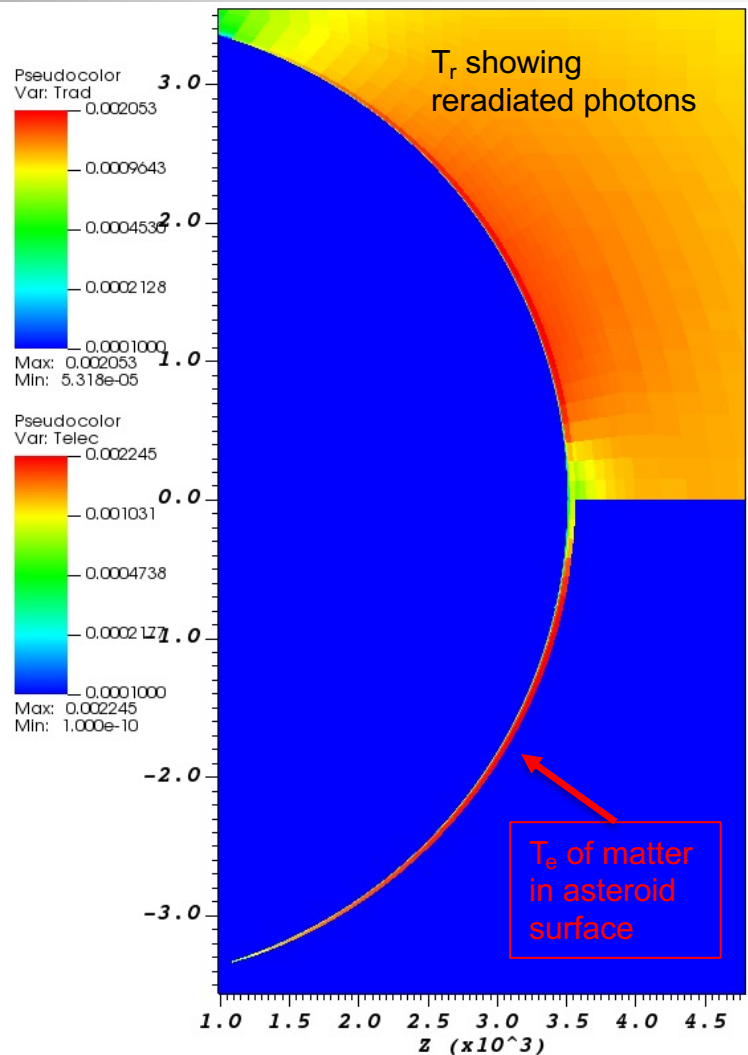
Ejected material

Energy escaping through asteroid surface

Escaping spectrum

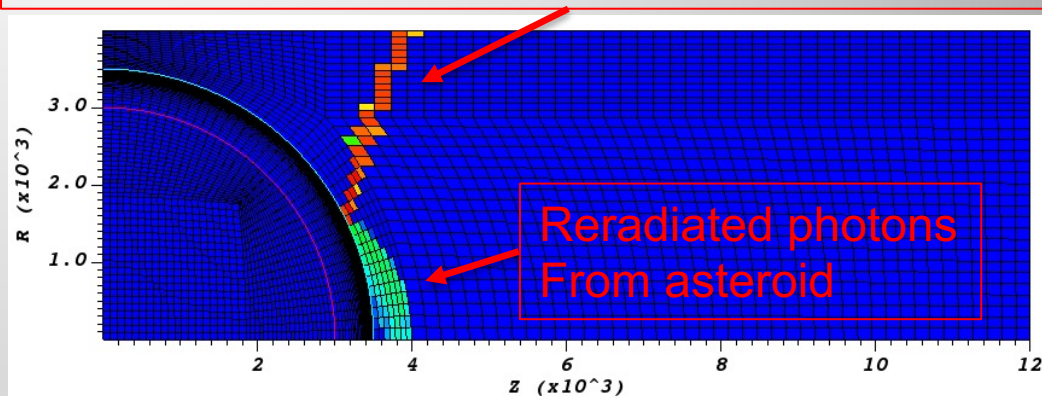


2D simulations provide more realistic exploration of deposition as a function of angle



Source photons

- The computational photons have exact positions on a spherical shell
- The jaggedness is an artifact of the coarse vacuum zoning



- $\frac{1}{2}$ of 35 m asteroid on an axisymmetric mesh
- Source is 1 kiloton, 85 m from surface
 - Spectrum = 1 keV Planckian
- 200 groups in $[3 \times 10^{-3}, 1000]$ keV log-spaced
- 20719 zones; sizes in $[10^{-6}, 100]$ cm
- 10^8 computational photons
- Materials = SiO₂, Fe, H₂O, Forsterite
- Simulations take ~ 1 Week on 144 2.1 MHz procs
- Hydrodynamics is Lagrangian
 - Mesh moves with the material

Radiation hydrodynamics simulations using IMC will contribute to asteroid deflection modeling

- We are currently running radiation hydrodynamics calculations in 1 and 2D
 - These expensive calculations model absorption and reemission, shock physics, and asteroid momentum
- These simulations allow us to characterize energy deposition with relevant physics
- We are investigating whether we can use that deposition in hydro-only calculations and still obtain accurate results for momentum coupling
 - These simulations ignore radiation transport but are much faster

A derivation of FLD with MMC

1) $\frac{\partial E_L}{\partial t} + \frac{\partial F_{L,i}}{\partial x_i} = c\sigma_a aT^4 - c\sigma_a E_F - \sigma_t \frac{v_i}{c} F_{F,i}$ Energy conservation in lab frame: $\nabla_a T_{rad}^{a0} = g_L^0$
 with $g_L^0 = g_F^0 + v_i g_F^i$, $g_F^0 = c\sigma_a aT^4 - c\sigma_a E_F$ and $g_F^i = -\frac{1}{c}\sigma_t F_F^i$ [See [2], Eqs.(6.31)—(6.38)]

2) $E_L = E_F + 2\frac{v_i}{c^2} F_{F,i} \approx E_F$ since we will drop $\frac{1}{c} \frac{\partial F_F}{\partial t}$ Express lab frame radiation quantities in fluid frame to $O(v/c)$ via Lorentz transformation [2] Eq.(6.30)
 $F_{L,i} = F_{F,i} + v_i E_F + v_j P_{F,ij} + O\left(\frac{v}{c}\right)$

3) $P_{F,ij} \equiv \frac{1}{c} \int_{4\pi} I_F \Omega_i \Omega_j d\Omega \approx \frac{1}{3} E_F \delta_{ij}$ assuming $I_F = \frac{1}{4\pi} (cE_F + \Omega_F \cdot F_F)$ I_F is weakly anisotropic

4) $F_F = -\mathcal{L}c \frac{1}{3\sigma_t} \frac{\partial E_F}{\partial x_{F,i}} \approx -\mathcal{L}c \frac{1}{3\sigma_t} \frac{\partial E_F}{\partial x_i}$ Flux ansatz in fluid frame and $\frac{\partial}{\partial x_{F,i}} = \frac{\partial}{\partial x_i} + \frac{v_i}{c^2} \frac{\partial}{\partial t}$ with $\mathcal{L} \in [0, 1]$ the flux limiter, used in $\frac{\partial F_{L,i}}{\partial x_i}$ term

5) $F_{F,i} = -c \frac{1}{3\sigma} \frac{\partial E}{\partial x_i}$ **Inconsistent!** Flux ansatz in fluid frame without the flux limiter, used in $\sigma_t \frac{v_i}{c} F_{F,i}$ term

Steps 1-5 finally yield the standard form of the diffusion equation with MMC

$$\frac{DE}{Dt} - \frac{\partial}{\partial x_i} \mathcal{L} \frac{1}{3\sigma_t} \frac{\partial E}{\partial x_i} + \frac{4}{3} E \frac{\partial v_i}{\partial x_i} = c\sigma aT^4 - c\sigma_a E$$

Eq.(11.9) in [2],
Eq.(7.18) in [6]

References

- [1] G.C. Pomraning, *Equations of Radiation Hydrodynamics*, in: D. ter Harr (Ed.), *International Series of Monographs in Natural Philosophy*, vol. 54, Pergamon, New York, 1973.
- [2] J.I. Castor, *Radiation Hydrodynamics*, Cambridge University Press, New York, 2007
- [3] Mihalas and Weibel-Mihalas, *Foundations of Radiation Hydrodynamics*, Oxford University Press, Oxford, 1984.
- [4] J. R. Buchler, Radiation Transfer in the Fluid Frame, *JQSRT* 30 No.5 (1983) 395–407.
- [5] R. B. Lowrie, D. Mihalas, J. E. Morel, Comoving-frame radiation transport for nonrelativistic fluid velocities, *JQSRT* 69 (2001) 291–304.
- [6] R.L. Bowers and J. R. Wilson, *Numerical Modeling in Applied Physics and Astrophysics*, Jones and Bartlett, Boston, 1991.

7th IAA Planetary Defense Conference

26-30 April 2021, Online Event

Hosted by UNOOSA in collaboration with ESA



Q&A

Session 7a: Deflection & Disruption Testing



7th IAA Planetary Defense Conference

26-30 April 2021, Online Event

Hosted by UNOOSA in collaboration with ESA



Break

Up next: Session 8a - Mission & Campaign Design

